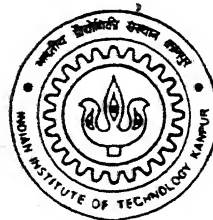# NAVIER-STOKES COMPUTATIONS FOR TWO-DIMENSIONAL HYPERSONIC FLOW

By

SHAILENDRA MISHRA

DEPARTMENT OF AEROSPACE ENGINEERING

INDIAN INSTITUTE OF TECHNOLOGY, KANPUR

DECEMBER, 1998

NAVIER-STOKES COMPUTATIONS FOR TWO-DIMENSIONAL HYPERSONIC FLOW

A Thesis Submitted

in Partial Fulfillment of the Requirements

for the Degree of

Master of Technology

by

SHAILENDRA MISHRA

to the

DEPARTMENT OF AEROSPACE ENGINEERING
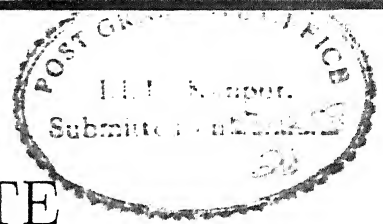
INDIAN INSTITUTE OF TECHNOLOGY KANPUR

December 1998

CERTIFICATE

It is certified that the work contained in the thesis entitled **Navier-Stokes Computations for Two-Dimensional Hypersonic Flow**, by **Shailendra Mishra**, has been carried out under my supervision and that this work has not been submitted elsewhere for a degree.

Dr. Ashish Tewari

Assistant Professor

Department of Aerospace Engineering

Indian Institute of Technology

Kanpur

December, 1998

Dedicated To

My Respected Parents
Smt. Chandra Prabha Mishra
And
Shri M. P. Mishra

Acknowledgement

At first I would like to thank my learned supervisor Dr. Ashish Tewari, who has been constant source of inspiration for me. I realise how important was his advice to do things fast when I used to slow down and I feel grateful to him for his co-operation for doing a good thesis in time. It will be an injustice if I do not mention the course "Introduction to Hypersonic Flows and Transatmospheric Flight" which he handled .

I thank Dr. D. P. Mishra who helped me a lot in my thesis work. He used to give useful suggestions and he also found time in discussing other topics of interest. I also thank Dr. T. K. Sengupta, Dr. A. K. Gupta and Dr. A. K. Ghosh who handled various courses during our first semester and gave a good foundation in Aerospace Engineering.

I found Rajesh and Prasanth as friends ready to help at any time. This page will be insufficient to thank them. But more than their help, the fun we had together in Hall 5 will be something I will cherish throughout my life. My brother Narendra was with me for the past one year and his presence made me feel homely and he used to be a source of inspiration. Venu and Raju were two other good friends whom I would like to remember here. I spent some nice unforgettable times with them. I also remember Bhaskar, Crao, Vinay, NKSingh and Kapil who were good friends. The list of friends is too long to mention here, but I will recall some names like Gyanendra, Ramu, Avinash, Sharad, Sagar, Aswini, Amit, Naresh, Abha and Ajay Kumar.

My parents and my elder brother Devendra though not physically present in this campus, used to inspire me through letters and their prayers. I conclude this page by dedicating this work to them because I am in this position today only due to their encouragement and prayers.

Abstract

The hypersonic viscous flow over a flat plate at zero angle of attack and wedge is determined by solving Navier-Stokes equations, using a time-marching technique. The steady state solution is attained asymptotically. The computation is performed in a rectangular domain. The method used for solving these equations is the explicit MacCormack finite difference scheme. This is a predictor-corrector scheme which is second order accurate. Shock-capturing method has been used where the location of the shock is obtained as a steady state solution without having an apriori knowledge about it. A code has been developed which generates numerical solution for any given Mach number. Detailed results for Mach numbers 4, 8 and 12 are presented and compared with existing results. The results obtained in this case have also been compared with those obtained from boundary layer equations and Newtonion approximations which shows that the coefficient of pressure on the body comes closer to the Newtonian approximation with increase in Mach number. Effect of number of grid points in domain on the result has been analysed. Results from both uniform and non-uniform grids have been obtained and compared. Reduction in coefficient of pressure and friction coefficient with Mach number has been observed. In addition to this it has been observed that the rate of increase in shock-wave strength for a wedge is higher than that for a flat plate. It has been observed from the results obtained that the strength of the shock wave increases and shock layer thickness decreases with increase in Mach number, as expected. In addition to this increase in strength of shock wave with increase in wedge angle has also been observed.

Contents

List of Figures

Nomenclature

c_f	-coefficient of friction
c_H	-Stanton number
c_p	-coefficient of pressure
e	-internal energy $(Joule)$
$\mathbf{E}$	- matrix containing all x derivative terms
E_t	-total energy per unit volume $(Joule/m.^3)$
$\mathbf{f}$	-acceleration vector $(m/sec.^2)$
$\mathbf{F}$	- matrix containing all y derivative terms
f_x, f_y, f_z	-acceleration along x, y and z direction respectively $(m/sec.^2)$
g	-acceleration due to gravity $(m/sec.^2)$
i, j	-grid point numbers along y and x axes respectively
$\mathbf{i, j, k}$	-unit vectors along x, y and z directions
k	-coefficient of thermal conductivity $(Watt/m/K)$
K	-coefficient of bulk viscosity $(Nsec/m.^2)$
K_f	-fudge factor
Kn	-Knudsen number
M	-Mach number
n	-number of time steps
p	-pressure $(N/m.^2)$
p_∞	-free stream pressure $(N/m.^2)$
Pr	-Prandtl number
Q	-total heat influx per unit volume $(Watt/m^3)$
$\mathbf{q}$	-rate of energy loss by convection per unit volume $(Watt/m.^3)$

r	-recovery factor
Re	-Reynold's number based on boundary layer properties
Re_x	-local Reynold's number
t	-time $(sec.)$
T_∞	-free stream temperature $(K.)$
$u_1,\ u_2,\ u_3$ and $u,\ v,\ w$	-velocity along x, y and z axes respectively $(m/sec.)$
$\mathbf{U}$	- matrix containing all time derivative terms
$\mathbf{V}$	-velocity vector $(m/sec.)$
V_∞	-free stream velocity $(m/sec.)$
$x,\ y$	-distance along x and y axis $(m.)$
y_n	-normalized y distance
λ	- mean free path $(m.)$
δ	-boundary layer thickness $(m.)$
α	-wedge angle $(degree)$
ρ_∞	-free stream density $(Kg/m.^3)$
$\Pi_{i,j}$	-stress tensor $(N/m.^2)$
ρ	-density $(Kg/m.^3)$
$\delta_{i,j}$	-Kronecker delta function
μ	-coefficient of viscosity $(Nsec/m.^2)$
μ'	-second coefficient of viscosity $(Nsec/m.^2)$
$\tau_{xx},\ \tau_{yy}$ and τ_{zz}	-normal stresses $(N/m.^2)$
$\tau_{xy},\ \tau_{yz}$ and τ_{xz}	-shear stresses $(N/m.^2)$
$\Delta x,\ \Delta y$	-grid spacing in x and y directions respectively $(m.)$
Δt	- time step $(sec.)$
γ	-specific heat ratio

Subscripts

∞	-free stream values
o	-standard values
$i,\ j$	-values at ith and jth points along y and x axis respectively
w	-value of the variable at the wall
e	-value at the edge of the boundary layer

Chapter 1

Introduction

1.1   Special Features of Hypersonic Flows

According to modern classification flow regimes are divided into sub-sonic flows(upto Mach Number 0.8), transonic flows (from Mach Number 0.8 to 1.2), supersonic flows (from Mach Number 1.2 to 5) and hypersonic flows (above Mach Number 5). Linearized theory can be used for studying subsonic and supersonic flows but the study of hypersonic flows is complicated, and requires special treatment because of the following reasons:

1. Shock layer is very thin for hypersonic flows. This thin shock layer can create some physical complications, such as the merging of the shock layer itself with a thick, viscous boundary layer growing from body surface. The shock-wave boundary-layer interaction becomes important at low Reynolds numbers.

2. Strong entropy gradients are generated in the nose region and the boundary layer along the surface grows inside this entropy layer and is affected by it. This entropy layer causes analytical problem due to simultaneous effect of boundary layer and entropy layer in the vicinity of the wall, while performing a standard

boundary layer calculation on the surface.

3. Boundary layer thickness in hypersonic flow is higher which can exert a major displacement effect on the inviscid flow outside the boundary layer. Due to the extreme thickness of the boundary layer flow the outer inviscid flow is greatly changed which in turn affects the growth of the boundary layer. This major interaction between the boundary layer and the outer inviscid flow is called viscous interaction. Viscous interaction affects the surface pressure distribution, hence lift, drag and stability of hypersonic vehicles. Moreover, skin friction and heat transfer are increased by viscous interaction.

   The boundary layer on a hypersonic vehicle is so thick that it merges with shock wave. In this case the shock layer is treated as fully viscous and the conventional boundary layer analysis is abandoned.

4. Boundary layer and normal and nearly normal shock in the nose region cause high temperature in hypersonic flow, which makes the flow chemically reacting. High temperature chemically reacting flows can influence lift, drag, and moments on a hypersonic vehicle. However the most important dominant aspect of high temperature is the resultant high heat transfer rates to the surface. Aerodynamic heating dominates the design of the hypersonic vehicle.

   In addition, high-temperature causes ionization producing free electrons which absorb radio frequency radiation. This results in communication blackout i.e. no transmission of radio waves either to or from the vehicle. Therefore, the accurate prediction of electron density within the flow field is important.

5. Since some hypersonic vehicles, fly at or through the outer region of atmosphere they experience the effect of low density. With increase in altitude mean free path (λ) and similarity parameter governing density regime (Knudsen number $Kn = \lambda/L$), increase. Continuum Navier-Stokes equations are applied up to $Kn<0.2$. Slip effects are included in these equations when $Kn>0.03$. The effect of free molecular flow begins around a value of $Kn=1$ and extends out to the value of $Kn=\infty$. Hence the transitional regime is essentially contained between

2

0.03<Kn<1.

1.2   Solution Methods of Hypersonic Viscous Flow Problems

Various approaches have been applied for the solution of hypersonic viscous flow problem. Before the advent of computational fluid dynamics exact solutions of complete Navier-Stokes equations for practical problems were difficult. This is the reason of simpler viscous flow solutions. The approximations used at that time involved separate calculations of the boundary layer and outer inviscid flow, and then a coupling of these separate calculations to take into account the viscous interaction. The weak and strong interaction serve a useful purpose in providing convenient correlations and predictions based on approximate theory. By a suitable order of magnitude reduction of Navier-Stokes equations boundary layer equations are obtained. The compressible boundary layer equations are the same for all flow regimes i.e subsonic, supersonic and hypersonic (neglecting high temperature effects). Various methods have been introduced to solve boundary layer equations.

1. The *difference-differential method* gives an exact solution of the general boundary layer equation. Smith and Clutter [1] have successfully solved these equations. They have stated that meeting boundary conditions efficiently has been the most difficult part of the entire flow problem.

2. *Finite difference method* was suggested by Blottner [2], these are inherently faster and more accurate than the other methods. He solved these equations for multi component flow with finite chemical reaction. DiCristina has obtained experimental results for a sharp 8 degree cone at Mach Number 10 [3] . Stetson has shown the results at Mach Number 6 over a cone [4].

3

If we consider the entire flow as fully viscous and no partition between boundary and inviscid flow, the viscous interaction effect can be calculated exactly.

There are basically three approaches used to solve the fully viscous flow problem which provide every information about the flow such as shock shape, detailed flow variables between shock and body, skin friction, heat transfer, lift, drag, moments etc.

1. Viscous Shock Layer Technique

This technique was introduced by Davis [5] who derived a set of equations which approximate the Navier-Stokes equations and solved them for a viscous shock layer over a blunt body at hypersonic speed. An order of magnitude reduction was applied to the Navier-Stokes equations. The terms are kept in second order in $1/\sqrt{Re}$ (Re = Reynolds number) to obtain the governing equations. Since these equations are parabolic hence downstream marching finite difference method is used. This method has found wide application to chemically reacting viscous flow.

2. Parabolized Navier-Stokes Solutions

This approach uses equations which contain more terms than the the viscous shock layer equations and hence more accurate but are not as accurate as the full Navier-Stokes equations. They are obtained from full Navier-Stokes equations (with all time derivatives zero) simply by neglecting all viscous terms which involve derivatives in the streamwise direction.

With two exceptions, these equations are a mixed system of parabolic-hyperbolic partial differential equations and hence are solved by a downstream marching procedure. The two exceptions are,

(a) In subsonic region, the pressure is constant in the direction normal to, the surface, equal to its value at the first grid point at which supersonic flow exists. This is done to preserve the parabolic nature of Parabolized Navier-Stokes (PNS) equations.

4

(b) The volumetric heating term, namely, can destroy the parabolic behaviour of the system. For flows where such volumetric heating does not occur, such a problem does not exist.

McWherler [6] has solved parabolized Navier-Stokes equations successfully in his work. He has calculated the flow over slender blunt nose cone at small angle of attack and compared the results with boundary layer solutions.

3. Full Navier-Stokes Solution

In this approach all the terms present in the Navier-Stokes equations are considered and is the ultimate viscous flow calculation. Hence this is used to obtain solution over a flat plate and a wedge. Navier-Stokes equations are a system of partial differential equations with a somewhat mixed hyperbolic, parabolic and elliptic behaviour. Due to their elliptic nature these equations cannot be solved by a downstream marching technique. Hence full Navier-Stokes equations have been solved by using a time dependent finite difference method. The major reason for using the time dependent method is that resulting unsteady Navier-Stokes equations are a mixed set of hyperbolic-parabolic equations for all subsonic and hypersonic flows. As a result, a very complicated flow field can be calculated as an initial value problem. An additional advantage is that since the complete Navier-Stokes equations are solved the shock wave, shear layer and a wall boundary layer are captured automatically in the solution without prior knowledge of their location or even existence.

1.3   Methods Available for Solution of Full Navier-Stokes Equations

Many numerical approaches are available for the solution of full Navier-Stokes equations using both implicit and explicit finite difference methods. Nearly all the methods are second order accurate in space and are first or second order accurate in time. The

explicit finite difference methods available are as follows:

1. *MacCormack Method*:-This method was introduced by MacCormack [7]. It uses forward difference for all special derivatives in predictor steps and backward difference in corrector steps. This eliminates any error due to one sided differencing. The method and it's application to the Navier-Stokes equations is given in Chapter 2.

2. *Hopscotch Method*:-It is an unconditionally stable method. It involves two sweeps through the mesh. Let i and j denote the number of grid points along x and y axis respectively and n be the time-step under consideration. For the first sweep the variables in the next time step e.g.: $u_{i,j}^{n+1}$ is computed at each grid point (for which i+j+n) is given by the simple explicit scheme and for the second sweep these variables are computed at each grid point(for which i+j+n) is odd by the simple implicit scheme.

3. *Leap Frog/Dufort -Frankel Method*

   This is a one step scheme and is first order accurate. In this method, time derivative is given by central-difference as shown below

   $$\left(\frac{\partial u}{\partial t}\right)_{i,j}^{n} = \frac{u_{i,j}^{n+1} - u_{i,j}^{n-1}}{2\Delta t}$$

   First order special derivative is given by central difference. This scheme is better suited for calculation of steady solutions, where time accuracy is not important.

4. *Allen-Cheng Method*

   This scheme is a first order accurate, predictor-corrector scheme. In predictor step, time derivative is given by the difference of predicted value in the next time step and value at the present time, while in corrector step it involves difference of corrected value in the next time step and the present value. This method allows larger time steps when viscosity is large.

5. *Lax-Wendroff Method*

It is a second order accurate two step method. In the first step variables at the half of the next time are determined. In the second step the variables obtained in the first step are used to find them at the next time step.

When the methods other than MacCormack method are applied to the complicated compressible Navier- Stokes equations certain problems can arise. For example the mixed derivative terms can create a problem for the Hopscotch method. If these terms are differenced in the usual manner the Hopscotch method is no longer explicit since a matrix inversion is required. All the above methods except the Lax-Wendroff scheme are first order accurate in time and so they cannot be used to accurately calculate the time evaluation of the time field. Being one of the better methods Mac-Cormack method is used to solve the problem.

1.4   Assessment of Existing Literature

Initially approximate solutions were derived for hypersonic flows .For a tangent cone, one pressure approximation was given by Hays and Probstein [8] using constant density approximation and Maurice [9] derived a simple, approximate solution for a cone. Daty and Maurice [10] obtained an approximate analytical solution by means of constant density approximation, for hypersonic flow past an inclined cylinder.

As stated earlier, there are various approaches which constitute the hypersonic viscous flow problem, but the solution of full Navier-Stokes equation is the exact solution. An attempt has been made in the succeeding paragraphs to identify the major steps and advances in the field of hypersonic viscous flow problem.

Work in this field started with the introduction of various methods to solve the boundary layer equation, since before the advent of computational fluid dynamics it

was not possible to solve the full Navier-Stokes equations. The pioneering work of Moretti and Abett[11] gave a time dependent computational method for blunt-body flows. The computation was performed for shock layer only, assuming shock layer is a discontinuous surface, dependent on time. Results for 2-D blunt bodies and for axisymmetric ones were obtained and compared with experimental data.

As an extension of his work, MacCormack [12] gave a numerical method for solving the equations of compressible viscous flows. This method is second order accurate in space and time, unconditionally stable, preserves conservation form, requires no block or scalar tridiagonal inversions, and thus more efficient than the existing methods. The validity of the method was checked by externally generating shock wave incident upon boundary layer on a flat plate.

After introduction of viscous shock layer technique by Davis[5] Horstman [13] gave solution for hypersonic/turbulent boundary layer interaction flows. Lind and Lewis [14] studied unsteady characteristics of shock-wave interaction (for which the peak pressure, heat transfer rate and surface pressure distributions are sensitive to upstream thermodynamic flow conditions, shock length and Mach number) at Mach Number 8 using a time accurate scheme for solving the thin layer approximation to the two dimensional Navier-Stokes equations. They showed by calculations that the peak surface pressure, the impingement location of the supersonic jet and the time required for the development of the interaction are strong functions of the impinging shock, location. For a range of impinging shock location of interaction is found to be unsteady.

Gupta et al. [15] presented numerical solutions from the steady viscous shock-layer equations for the hypersonic laminar and turbulent flow of a perfect gas over long slender bodies. Kussoy and Horstman[16] presented experimental data for two three dimensional intersecting shock wave/turbulent boundary layer interaction flows at Mach number 8.3. Gupta et al. [17] presented a solution procedure that improved the computational efficiency of the viscous shock layer technique, especially for long slender

bodies. Cheatwood and DeJarnette [18] had developed an axisymmetric approximate method which could calculate laminar(perfect gas, non-equilibrium, equilibrium) and turbulent(perfect gas and equilibrium) viscous hypersonic flow over blunt nosed body. Simplified form of viscous shock layer equations were used. Results were obtained for flow over analytic body shapes. Surface heat transfer and pressure predictions were generally in good agreement with viscous shock layer results.

Bigdeli et.al. [19] used turbulent viscous interaction theory to understand the hypersonic flow past an expansion corner. The paper of Luca and Cardone [20] dealt with an experimental investigation carried out to study some aspects of shock/boundary layer interactions in normal two dimensional hypersonic wedge flow over flat-plate/ramp configuration.

The parabolized Navier-Stokes (PNS) equations have also been used to successfully compute the 3-D hypersonic viscous flow over variety of body shapes at angle of attack. In this series Tannehil et.al. [21] had developed a parabolized Navier-Stokes code to compute the steady supersonic viscous flow around arbitrary body shot at high angle of attack. A nonorthogonal 3-D co-ordinate frame was employed which permitted the code to march with solution surfaces. The code was used to calculate the laminar flow over a slab delta wing with 70 degree sweep at angles of attacks upto 41.5 degrees and Mach Numbers of 6.8 and 9.6. Barnett and Davis [22] described a procedure for the calculation of strong viscous inviscid interactions in 2-D laminar supersonic interactive flows with and without separation. The equations solved were parabolized Navier-Stokes equations. Results were obtained for flow past flat plate related bodies

.

Dash et.al. [23] described parabolized Navier-Stokes models under development for the analysis of 3-D supersonic and subsonic propulsive jet mixing problem, and Kimmel et.al. [24] assumed the stability of boundary layers on sharp nosed cones with elliptical cross sections using linear stability theory and cross flow correlations. PNS computer codes were used to calculate the mean flow about cones with various

eccentricities at a free stream Mach Number 7.95 and a Reynolds Number $3.3 \times 10^6 m^{-1}$.

For complete and exact solution of hypersonic viscous flow problem full Navier-Stokes equations have been solved. In this context Kumar and Salas [25] obtained Euler and Navier-Stokes solutions of the supersonic shear flow past a circular cylinder. The results obtained indicate that the Euler equations may correctly predict certain high Reynolds number separation phenomena in flows with a natural inviscid vorticity source. Hung and Timothy numerically solved the compressible Navier-Stokes equations for hypersonic flow over a 3-D ramp with a narrow expansion slot. They had shown that wall cooling reduces the thickness of boundary layer and hence increases the flow expansion substantially. Hung and Barth [26] solved compressible Navier-Stokes equations for hypersonic flow over a three dimensional ramp with a narrow expansion slot. Solutions were obtained for various wall temperatures and slot widths.

For the very first time Shang and Scherr[27] presented the numerical simulation of the flow-field around a complete lifting body configuration utilizing the Reynolds averaged Navier-Stokes equations. The numerical solutions generated for the experimental aircraft X24C-10D, at a Mach Number of 5.95, exhibited accurate prediction of detailed flow properties and integrated aerodynamic coefficients as well. Zoby et.al. [28] in their technical notes gave an idea about hypersonic non-equilibrium viscous solutions over slender bodies.

Oberkampf and Aeschliman [29] presented aerodynamic force and moment measurements and flow visualization results for a hypersonic vehicle configuration at Mach Numbre 8 and after that Walker[30] developed parabolized and Navier-Stokes code to predict flow field solution around a hypersonic vehicle. Aerodynamic forces and moment predictions from the codes are compared with experimental data obtained in Ref.[29].Lockman et.al. [31] established a benchmark experimental database for a generic hypersonic vehicle shape for validation and/or calibration of advanced computational fluid dynamics computer codes. They included results from the comprehensive

test program conducted in the NASA Ames 3.5 ft wind tunnel for a generic all-body hypersonic aircraft model. Computational results obtained were compared with experimental results. Papuceuoglu [32] experimentally investigated the high heat transfer rates and flow patterns in the viscinity of 90 degree axial corner at a Mach Number of 6 and a Reynolds number range from 7 to 22.5×10^6.

Tai and Kao [33] developed a full Navier-Stokes code for predicting the aerodynamic properties of slender bodies. An explicit upwind flux-difference split scheme combined with a multistage method was implemented for solving the axisymmetric full Navier-Stokes equation. Experimental data were found to be in good agreement with the code predictions.

Apart from the works stated above some other works have also been done in the field of hypersonic viscous flow, e.g.: Kim et.al. [34] obtained numerical solutions for the Navier-Stokes equations for laminar hypersonic flow around a flat based projectile using perfect gas, equilibrium air and non-equilibrium air models. The effects of different gas models were investigated for a free stream condition of Mach Number 20 and at an altitude of 73 km. Both implicit and explicit integration schemes were used. Morgenstern and Chokami [35] solved time dependent compressible Navier-Stokes equations for hypersonic flow over a cavity.

Mallett et.al. [36] implemented a kinetic theory based Navier-Stokes solver on a parallel super computer to study the leeward flow-field of a blunt nosed delta wing at 30 degree incidence at hypersonic speed. Computational results were presented for a series of grids for both inviscid and laminar viscous flow. Kopriva [37] presented steady solutions of high speed viscous flow over blunt bodies. The region within a shock layer was divided into subdomains so that internal layers can be well resolved. At interface between subdomains, the advective terms were upwinded and viscous terms were treated by a penalty method. The method was applied to various hypersonic flows. Results were compared with the experimental data and to a finite difference solution.

Habashi et.al. [38] presented a finite element segregated method for 2-D hypersonic thermochemical non-equilibrium flow, with emphasis on efficiently resolving shock-wave by mesh adaptation. The governing equations were decoupled into three systems of partial differential equations, gas dynamic, chemical and vibrational systems and then solved in a sequential manner.

1.5 Scope of the Work

The results obtained in the work give the exact value of skin-friction coefficient and the rate of heat transfer at the surface, which are useful parameters for the selection of materials, design, calculation of thrust and rate of cooling required for hypersonic vehicles (e.g. space vehicles, missiles etc.).

Hence the work done is very useful in the space and missile programme. Results may be helpful in the exact calculation of the bluntness required for the nose of a missile or spacecraft (which decides the temperature gradient in that region) and optimize the drag. The problem finds its important application in the analysis of effect of aerothermodynamics of the flow on the structural dynamics of the body. As observed at higher Mach numbers temperature and pressure on the body are very high. Since high temperature reduces the stiffness of the structure, both temperature and pressure at hypersonic speed causes large deflection on the body (wings of the aircraft). Thus limit of the speed can exactly be defined by considering this effect.

The present problem can be extended to a three-dimensional problem by considering the third spatial parameter of the Navier-Stokes equation.

Chapter 2

Problem Statement and Governing Equations

2.1   Problem Statement

Consider a viscous fluid flowing steadily at a hypersonic speed over a wedge of angle α. To predict the macroscopic behavior a domain has been defined. In flow boundary of the domain is at leading edge of the wedge. The lower boundary is at the surface of the wedge while upper boundary is at a distance of 5δ (δ=boundary layer thickness and is given by the expression $\delta = \frac{5L}{\sqrt{Re_x}}$, where L is length of plate) from the wedge and parallel to it. The problem is confined to the face of the wedge and does not include backward facing step at the trailing edge of the wedge.

A cartesian coordinate system is chosen. x and y distances are measured by considering leading edge of the wedge as origin, wedge as x axis and inflow boundary as y axis. Flow approaches with a uniform velocity V_∞ The components of velocity in x and y directions are u and v respectively. It is assumed that the flow is two dimensional.

2.2 Governing Equations

2.2.1 Continuity Equation

The conservation of mass applied to a prefect gas passing through an infinitesimal, fixed control volume yields the following equation of continuity

$$\frac{\partial \rho}{\partial t} + \nabla \cdot (\rho \mathbf{V}) = 0 \tag{2.1}$$

For a cartesian coordinate system, where u, v, w represent the x, y, z components, respectively, of velocity vector $\mathbf{V}$ and ρ represents density, the above equation becomes

$$\frac{\partial \rho}{\partial t} + \frac{\partial (\rho u)}{\partial x} + \frac{\partial (\rho v)}{\partial y} + \frac{\partial (\rho w)}{\partial z} = 0 \tag{2.2}$$

2.2.2 Momentum Equation

Newton's second law applied to a prefect gas passing through an infinitesimal, fixed control volume yields the following momentum equation

$$\frac{\partial (\rho \mathbf{V})}{\partial t} + \nabla \cdot \rho \mathbf{V} \mathbf{V} = \rho \mathbf{f} + \nabla \cdot \Pi_{i,j} \tag{2.3}$$

where $\rho \mathbf{f}$ is the body force per unit volume which is mainly the gravitational force, hence

$$\rho \mathbf{f} = \rho \mathbf{g} \tag{2.4}$$

and $\nabla \cdot \Pi_{i,j}$ represents the surface forces per unit volume. In this equation $\rho \mathbf{V} \mathbf{V}$ is a tensor so that $\nabla \cdot \rho \mathbf{V} \mathbf{V}$ is not a simple divergence. This can be explained as

$$\nabla \cdot \rho \mathbf{V} \mathbf{V} = \rho \mathbf{V} \cdot \nabla \mathbf{V} + \mathbf{V} \left(\nabla \cdot \rho \mathbf{V} \right) \tag{2.5}$$

Putting expression for $\nabla \cdot \rho \mathbf{V} \mathbf{V}$ in Equation 2.5 and simplification by using the continuity equation gives

$$\rho \frac{D \mathbf{V}}{Dt} = \rho \mathbf{f} + \nabla \cdot \Pi_{i,j} \tag{2.6}$$

14

where $\rho \mathbf{f}$ is the body force per unit volume which is mainly the gravitational force.

These forces are applied by external stresses on the fluid element. The stresses consist of normal stresses and shearing stresses and are represented by the components of the stress tensor $\Pi_{i,j}$, which can be expressed in compact tensor notation as

$$\Pi_{i,j} = -p\delta_{i,j} + \mu \left(\frac{\partial u_i}{\partial x_j} + \frac{\partial u_i}{\partial x_i} \right) + \delta_{i,j}\mu' \frac{\partial u_k}{\partial x_k} \quad (i,j,k = 1,2,3) \tag{2.7}$$

where p is pressure and $\delta_{i,j}$ is Kronecker delta function ($\delta_{i,j} = 1$ if i=j and $\delta_{i,j} = 0$ if i$\neq$ j);u_1, u_2, u_3 represent the three components of the velocity vector V;x_1, x_2, x_3 represent the three components of the position vector;μ is the coefficient of dynamic viscosity and μ' is the second coefficient of viscosity.μ and μ' are related by the expression

$$K = \frac{2}{3}\mu + \mu' \tag{2.8}$$

where K is the coefficient of bulk viscosity and is negligibly small except in the study of the structure of shock waves and in absorption and attenuation of acoustic waves, hence

$$\mu' = -\frac{2}{3}\mu \tag{2.9}$$

Thus equation can be written as

$$\rho\frac{D\mathbf{V}}{Dt} = \rho\mathbf{f} - \nabla p + \frac{\partial}{\partial x_j} \left[\mu \left(\frac{\partial u_i}{\partial x_j} + \frac{\partial u_i}{\partial x_i} \right) - \frac{2}{3}\delta_{i,j}\mu \frac{\partial u_k}{\partial x_k} \right] \tag{2.10}$$

or

$$\rho\frac{D\mathbf{V}}{Dt} = \rho\mathbf{f} - \nabla p + \frac{\partial}{\partial x_j} \left[\tau_{i,j} \right] \tag{2.11}$$

where $\tau_{i,j}$ is the viscous stress tensor.

Writing equation for a cartesian coordinate system, obtaining them in conservation law form and assigning $u_1 = u$, $u_2 = v$, $u_3 = w$ gives

$$\frac{\partial (\rho u)}{\partial t} + \frac{\partial}{\partial x} \left(\rho u^2 + p - \tau_{xx} \right) + \frac{\partial}{\partial y} \left(\rho uv - \tau_{xy} \right) + \frac{\partial}{\partial z} \left(\rho uw - \tau_{xz} \right) = \rho f_x$$

$$\frac{\partial (\rho v)}{\partial t} + \frac{\partial}{\partial x} \left(\rho uv - \tau_{xy} \right) + \frac{\partial}{\partial y} \left(\rho v^2 + p - \tau_{yy} \right) + \frac{\partial}{\partial z} \left(\rho uw - \tau_{yz} \right) = \rho f_y \tag{2.12}$$

$$\frac{\partial (\rho w)}{\partial t} + \frac{\partial}{\partial x} \left(\rho uw - \tau_{xz} \right) + \frac{\partial}{\partial y} \left(\rho vw - \tau_{yz} \right) + \frac{\partial}{\partial z} \left(\rho w^2 + p - \tau_{zz} \right) = \rho f_z$$

where the components of the viscous stress tensor $\tau_{i,j}$ are given by

$$\tau_{xx} = \frac{2}{3}\mu\left(2\frac{\partial u}{\partial x} - \frac{\partial v}{\partial y} - \frac{\partial w}{\partial z}\right)$$

$$\tau_{yy} = \frac{2}{3}\mu\left(2\frac{\partial v}{\partial y} - \frac{\partial u}{\partial x} - \frac{\partial w}{\partial z}\right)$$

$$\tau_{zz} = \frac{2}{3}\mu\left(2\frac{\partial w}{\partial z} - \frac{\partial u}{\partial x} - \frac{\partial v}{\partial y}\right)$$

$$\tau_{xy} = \mu\left(\frac{\partial u}{\partial y} + \frac{\partial v}{\partial x}\right) = \tau_{yx}$$

$$\tau_{xz} = \mu\left(\frac{\partial w}{\partial z} + \frac{\partial u}{\partial z}\right) = \tau_{zx}$$

$$\tau_{yz} = \mu\left(\frac{\partial v}{\partial z} + \frac{\partial w}{\partial y}\right) = \tau_{zy}$$

$$(2.13)$$

and

$$\mathbf{f} = f_x\mathbf{i} + f_y\mathbf{j} + f_z\mathbf{k} \qquad (2.14)$$

where $\mathbf{i}$, $\mathbf{j}$ and $\mathbf{k}$ are unit vectors along x, y and z directions respectively.

2.2.3 Energy Equation

The first law of thermodynamics applied to a prefect gas passing through an infinitesimal, fixed control volume yields the following energy equation:

$$\frac{\partial E_t}{\partial t} + \nabla \cdot E_t\mathbf{V} = \frac{\partial Q}{\partial t} - \nabla \cdot \mathbf{q} + \rho\mathbf{f} \cdot \mathbf{V} + \nabla \cdot (\mathbf{\Pi_{i,j}} \cdot \mathbf{V}) \qquad (2.15)$$

where E_t is the total energy per unit volume given by

$$E_t = \rho\left(e + \frac{V^2}{2} + PotentialEnergy + \cdots\right) \qquad (2.16)$$

and e is the internal energy per unit mass. $\frac{\partial Q}{\partial t}$ in Equation (2.15) represents the rate of increase of the total energy per unit volume in the control volume while $\nabla.\mathbf{q}$ represents the rate of total energy lost by convection (per unit volume) through the

16

control surface. For cartesian coordinate system equation becomes

$$\frac{\partial E_t}{\partial t} - \frac{\partial Q}{\partial t} - \rho\left(f_x u + f_y v + f_z w\right) + \frac{\partial}{\partial x}\left(E_t u + pu - u\tau_{xx} - v\tau_{xy} - w\tau_{xz} + q_x\right)$$

$$+\frac{\partial}{\partial y}\left(E_t v + pv - u\tau_{xy} - v\tau_{yy} - w\tau_{yz} + q_y\right) + \frac{\partial}{\partial z}\left(E_t w + pw - u\tau_{xz} - v\tau_{yz} - w\tau_{zz} + q_z\right) = 0$$

$$(2.17)$$

where

$$\mathbf{q} = q_x \mathbf{i} + q_y \mathbf{j} + q_z \mathbf{k}. \qquad (2.18)$$

In terms of heat conduction

$$q_x = -k\left(\frac{\partial T}{\partial x}\right)$$

$$q_y = -k\left(\frac{\partial T}{\partial y}\right)$$

$$q_z = -k\left(\frac{\partial T}{\partial z}\right)$$

2.3 Vector Form of Equations

For consistent application of finite difference algorithm to the governing fluid dynamic equations, they are combined in compact form. The compressible Navier-Stokes equations in two dimensional cartesian coordinates without body force or external heat addition is expressed as

$$\frac{\partial \mathbf{U}}{\partial t} + \frac{\partial \mathbf{E}}{\partial x} + \frac{\partial \mathbf{F}}{\partial y} = 0 \qquad (2.19)$$

where $\mathbf{U}$, $\mathbf{E}$ and $\mathbf{F}$ are vectors given by

$$\mathbf{U} = \begin{bmatrix} \rho \\ \rho u \\ \rho v \\ E_t \end{bmatrix}$$

17

$$
\mathbf{E} = \begin{bmatrix} \rho u \\ \rho u^2 + p - \tau_{xx} \\ \rho uv - \tau_{xy} \\ (E_t + p)u - u\tau_{xx} - v\tau_{xy} + q_x \end{bmatrix}
$$

$$
\mathbf{F} = \begin{bmatrix} \rho v \\ \rho uv + p - \tau_{xy} \\ \rho v^2 + p - \tau_{yy} \\ (E_t + p)v - u\tau_{xy} - v\tau_{yy} + q_y \end{bmatrix}
$$

$$(2.20)$$

2.4 Initial and Boundary Conditions

For the final solution of the flow problem we need some initial values of the flow parameters to start with at time $t = 0$, the values are called initial conditions. Except as noted below, properties at each grid point are initialized as their respective free stream values. These initial conditions are

$$
\begin{aligned}
u &= V_\infty \cos \alpha \\
v &= -V_\infty \sin \alpha \\
p &= p_\infty \\
T &= T_\infty.
\end{aligned}
$$

$$(2.21)$$

After specifying these artificial initial conditions, suitable boundary conditions are specified. The boundary conditions applied are as follows:

1. At the leading edge of the plate, no-slip is enforced (i.e $u_{(0,0)} = v_{(0,0)} = 0.0$ and the temperature ($T_{(0,0)}$) and pressure ($p_{(0,0)}$) are assumed to be their respective free stream values.

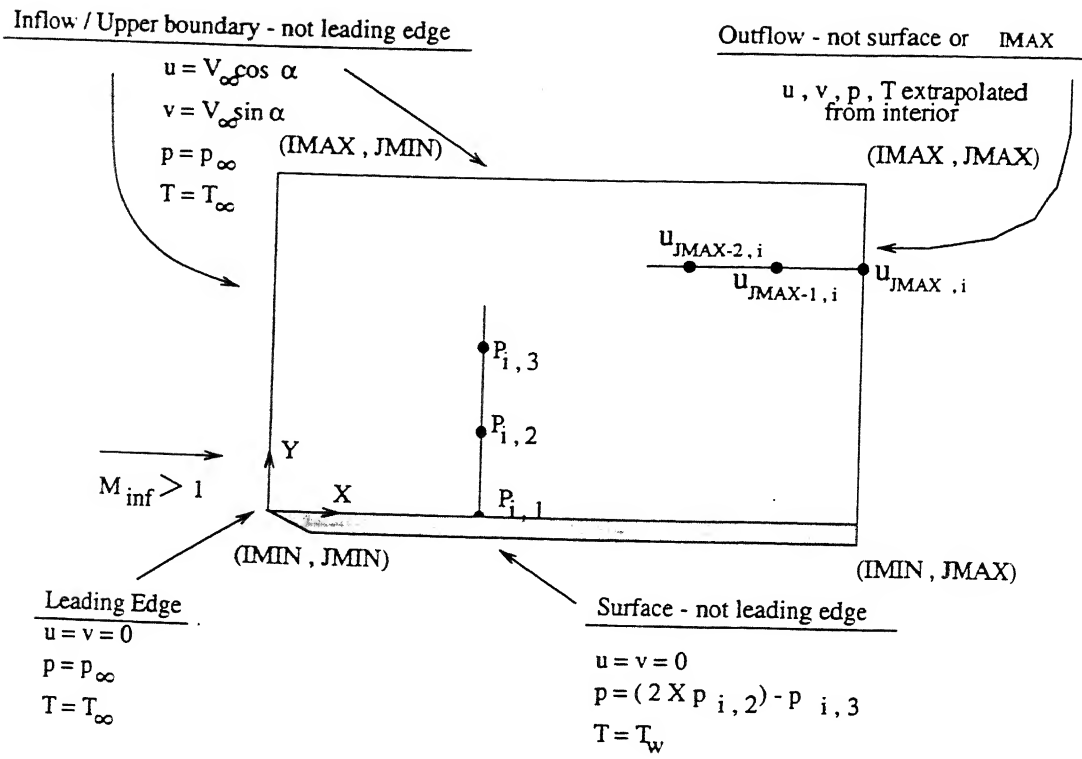2. At the inflow boundary (except the leading edge) and upper boundaries of the

18

$u = V_\infty \cos \alpha$

$v = V_\infty \sin \alpha$

$p = p_\infty$

$T = T_\infty$

(IMAX , JMIN)

u , v , p , T extrapolated
from interior

(IMAX , JMAX)

$u_{JMAX-2,i}$

$u_{JMAX-1,i}$

$u_{JMAX,i}$

$P_{i,3}$

$P_{i,2}$

Y

X

$M_{inf} > 1$

$P_{i,1}$

(IMIN , JMIN)

(IMIN , JMAX)

Leading Edge

$u = v = 0$

$p = p_\infty$

$T = T_\infty$

Surface - not leading edge

$u = v = 0$

$p = (2 \times p_{i,2}) - p_{i,3}$

$T = T_w$

Figure 2.1: Application of Boundary Condition

domain, the x-component of velocity, u, the y-component of velocity, v, temperature and pressure are assumed to be their free-stream values.

3. At the surface of the plate, no slip is specified on velocity($u = v = 0.0$). Temperature (except the leading edge) is assumed to equal to the wall temperature T_w. Pressure, (except the leading edge) is calculated at the wall by extrapolating from the values at the two points ($i = 1$ and $i = 2$) above the surface, as follows:

$$p_{(0,j)} = \left(2p_{(1,j)}\right) - p_{(2,j)} \tag{2.22}$$

4. All properties on the outflow boundary of the domain (not including $i = 0$ and $i = IMAX$) are calculated on the basis of an extrapolation from the two interior points, at the same j location. It is done as follows:

$$u_{(i,JMAX)} = \left(2u_{(i,JMAX-1)}\right) - u_{(i,JMAX-2)} \tag{2.23}$$

19

2.5 Calculation of Skin Friction Coefficient and Rate of Heat Transfer

2.5.1 Skin Friction Coefficient

From the value of u and v on the surface and at grid point just above the surface, shear stress τ_{xy} is calculated using relation

$$\tau_{xy} = \left[\mu \left(\frac{\partial u}{\partial y} \right) \right]_w$$

Now skin friction coefficient is calculated from

$$c_f = \frac{\tau_{xy}}{\frac{1}{2} \rho_\infty V_\infty^2}$$

For comparison with the results of boundary-layer equations c_f is calculated form

$$c_f = \frac{\tau_{xy}}{\frac{1}{2} \rho_e u_e^2}$$

where ρ_e and u_e are density and velocity u at the boundary-layer, i.e. at location when velocity profile begins to be vertical.

2.5.2 Rate of Heat Transfer

From the values of T and k on the surface and at the grid points just above the surface, rate of heat transfer is calculated form relation

$$q_w = \left[-k \left(\frac{\partial T}{\partial y} \right) \right]_w$$

Stanton number for comparison with the results of boundary-layer equations is calculated by the use of relation

$$c_H = \frac{q_w}{\rho_e u_e c_p \left(T_e + r \frac{u_e^2}{2 T_e} - T_w \right)}$$

where $r = \sqrt{Pr}$.

Chapter 3

Numerical Formulation and Solution Procedure

The finite difference method has been used in this work to solve the system of equations presented in Chapter 2, namely, Equation (2.2), (2.12) and (2.17). The principle used in this method is the conversion of partial differential equations to difference equations by the discretization of governing equations on a finite grid. The values of the flow variables are evaluated at each node and after each line step. The choice of the grid is very important for the accuracy of the grid.

3.1 Discretization of Derivatives

Each term in governing partial differential Equations (2.2), (2.12) and (2.17) can be written in a difference form using taylor series expansion approximation of variable around the ith node(as described in Appendix A). x axis is on the surface of the wedge and y axis on the inflow boundary.
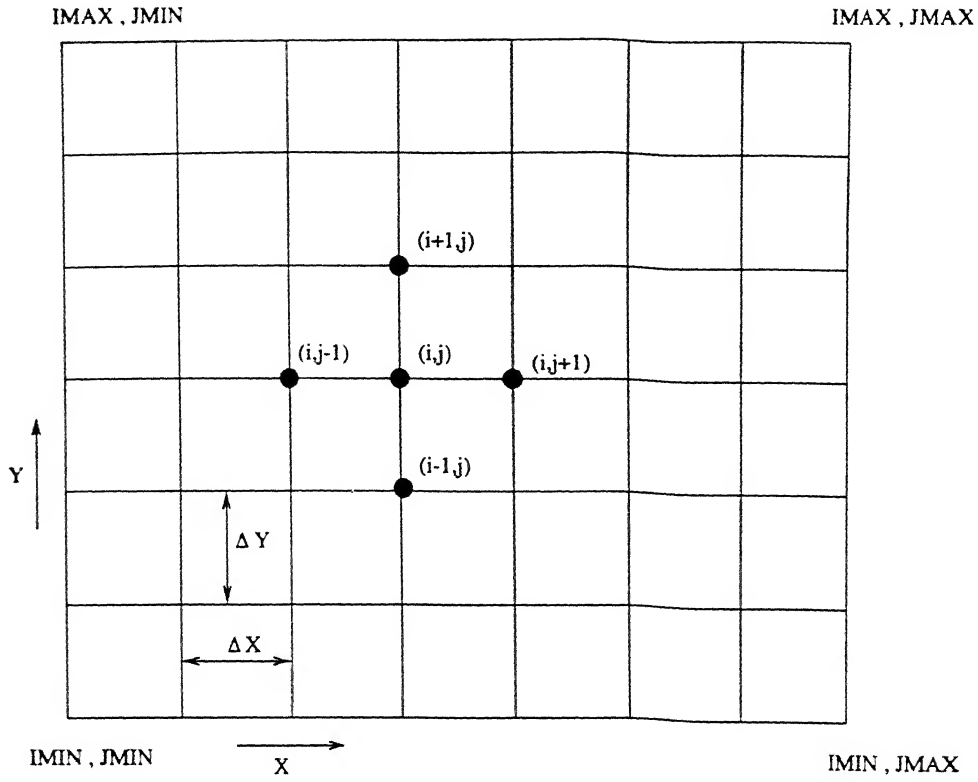
Figure 3.1: Finite Difference Grid Representation

$$\frac{\partial u}{\partial y}\Big|_i = \frac{u_{i+1} - u_i}{\Delta y} \qquad (Forward\ difference)$$

$$\frac{\partial u}{\partial y}\Big|_i = \frac{u_{i-1} - u_i}{\Delta y} \qquad (Backward\ difference)$$

$$\frac{\partial u}{\partial y}\Big|_i = \frac{u_{i+1} - u_{i-1}}{\Delta y} \qquad (Central\ Difference)$$

For an irregular grid:

$$\frac{\partial u}{\partial y}\Big|_i = \frac{u_{i+1} - u_i}{y_{i+1} - y_i} \qquad (Forward\ difference)$$

$$\frac{\partial u}{\partial y}\Big|_i = \frac{u_i - u_{i-1}}{y_i - y_{i-1}} \qquad (Backward\ difference)$$

$$\frac{\partial u}{\partial y}\Big|_i = \frac{u_{i+1} - u_{i-1}}{y_{i+1} - y_{i-1}} \qquad (Central\ difference)$$

22

3.2   Grid Generation

Since with the increase in the Mach number, shock layer thickness decreases and heat transfer, pressure distribution on the surface increases, it needs finer grids throughout the domain (if we use uniform grid) for higher Mach numbers. But large number of grid points in the domain increases the computational time. To overcome this problem, we can use non-uniform grid with small vertical spacing near the plate and relatively large vertical spacing away from the plate.

Both uniform and non-uniform grids have been used to obtain the results. For non-uniform grid non-uniformity in grid intervals is employed in y direction only while uniform intervals are used in x direction. Fig(3.2) shows the uniform and non-uniform grids respectively.

3.3   MacCormack Scheme

Writing the governing equations in the form

$$\frac{\partial \mathbf{U}}{\partial t} = -\frac{\partial \mathbf{E}}{\partial x} - \frac{\partial \mathbf{F}}{\partial y} \tag{3.1}$$

By means of Taylor series expansion the flow field variables are advanced at each grid point (i,j) in steps of time as

$$\mathbf{U}_{i,j}^{t+\Delta t} = \mathbf{U}_{i,j}^{t} + \left(\frac{\partial \mathbf{U}}{\partial t}\right)_{av} \Delta t \tag{3.2}$$

where once again $\mathbf{U}$ is a flow field variable (from the governing equations) assumed known at time t, either from initial conditions or as a result from the previous iteration
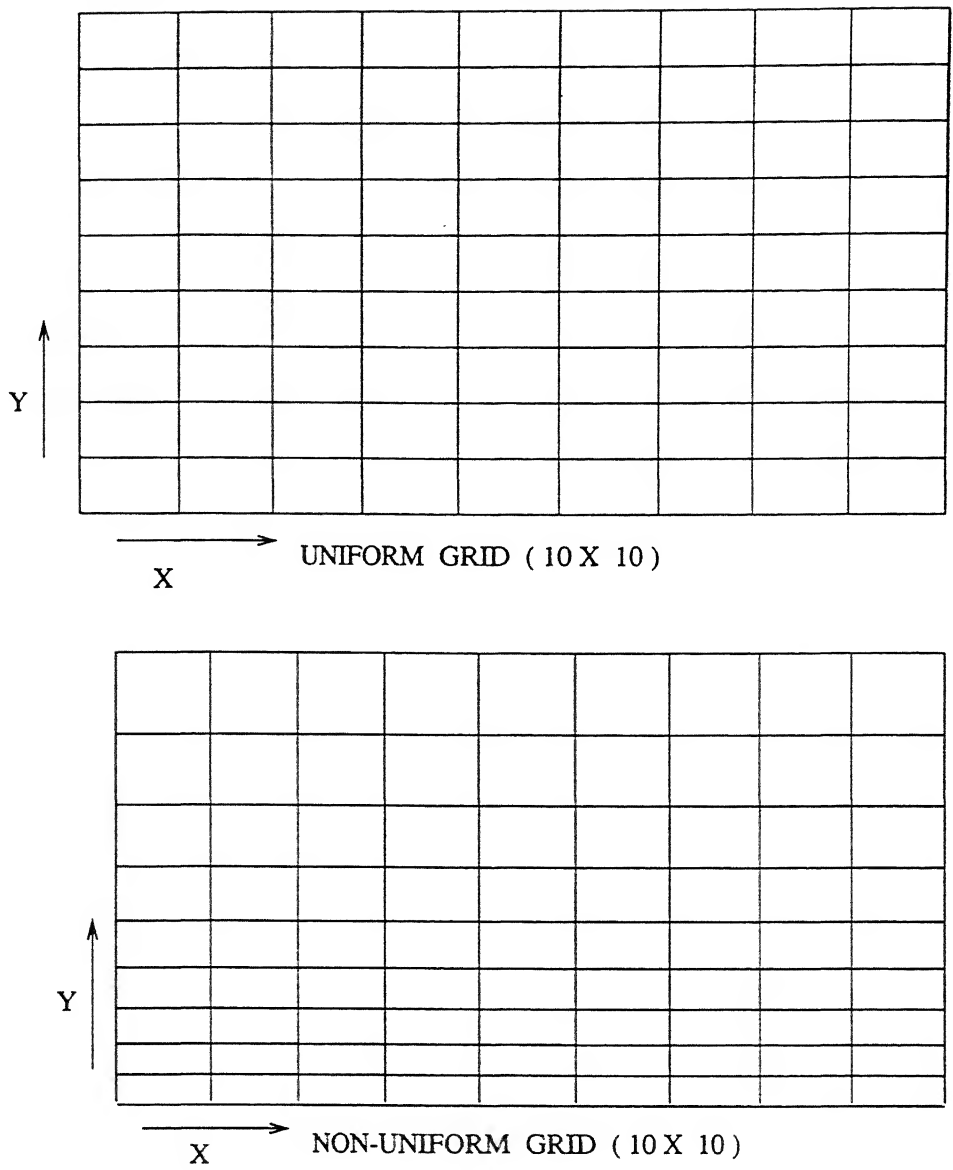
23

UNIFORM GRID (10 X 10)

NON-UNIFORM GRID (10 X 10)

Figure 3.2: Uniform and Non-Uniform Grid Geometry

in time. $\left(\frac{\partial U}{\partial t}\right)_{av}$ is defined as

$$\left(\frac{\partial U}{\partial t}\right)_{av} = \frac{1}{2}\left[\left(\frac{\partial U}{\partial t}\right)^{t}_{i,j} + \left(\frac{\partial \bar{U}}{\partial t}\right)^{t+\Delta t}_{i,j}\right] \tag{3.3}$$

To obtain a value of $\left(\frac{\partial U}{\partial t}\right)_{av}$ the following steps are followed.

1. $\left(\frac{\partial U}{\partial t}\right)^{t}_{i,j}$ is calculated using forward spatial differences on the right hand side of the governing equations from the known flow field at time t.

2. From Step 1, predicted values of the flow-field variables (denoted by bar) can be obtained at time $t + \Delta t$ as follows:

$$\bar{\mathbf{U}}_{i,j}^{t+\Delta t} = \mathbf{U}_{i,j}^{t} + \left(\frac{\partial \mathbf{U}}{\partial t}\right)_{i,j}^{t} \Delta t \tag{3.4}$$

Combining Step1 and Step2, predicted values are determined as follows:

$$\bar{\mathbf{U}}_{i,j}^{t+\Delta t} = \mathbf{U}_{i,j}^{t} - \frac{\Delta t}{\Delta x}\left(\mathbf{E}_{i+1,j}^{t} - \mathbf{E}_{i,j}^{t}\right) - \frac{\Delta t}{\Delta y}\left(\mathbf{F}_{i,j+1}^{t} - \mathbf{F}_{i,j}^{t}\right) \tag{3.5}$$

3. Using rearward spatial differences, the predicted values (from Step 2) are inserted into the governing equations such that the predicted time derivative $\left(\frac{\partial \bar{\mathbf{U}}}{\partial t}\right)_{i,j}^{t+\Delta t}$ can be obtained.

4. Finally substitute $\left(\frac{\partial \bar{\mathbf{U}}}{\partial t}\right)_{i,j}^{t+\Delta t}$ (from Step 3) into equation to obtain corrected second-order accurate values of $\mathbf{U}$ at time $t + \Delta t$. Hence combining Step3 and Step4 we get;

$$\mathbf{U}_{i,j}^{t+\Delta t} = \frac{1}{2}\left[\mathbf{U}_{i,j}^{t} + \bar{\mathbf{U}}_{i,j}^{t+\Delta t} - \frac{\Delta t}{\Delta x}\left(\bar{\mathbf{E}}_{i,j}^{t+\Delta t} - \bar{\mathbf{E}}_{i-1,j}^{t+\Delta t}\right) + \frac{\Delta t}{\Delta y}\left(\bar{\mathbf{F}}_{i,j}^{t+\Delta t} - \bar{\mathbf{F}}_{i,j-1}^{t+\Delta t}\right)\right] \tag{3.6}$$

Steps 1 to 4 are repeated until the flow-field variables approach a steady-state value; which is the desired steady-state solution.

In order to maintain second-order accuracy, the x-derivative terms appearing in $\mathbf{E}$ are different in the opposite direction to that used for $\frac{\partial \mathbf{E}}{\partial x}$, while the y derivative terms are approximated with central differences. Similarly, the y-derivative terms appearing in $\mathbf{F}$ are differenced in opposite direction to that used for $\frac{\partial \mathbf{F}}{\partial y}$, while the x-derivative terms in $\mathbf{F}$ are approximated by central differences. Hence for predictor step terms appearing in $\mathbf{E}$ are discretized as

$$\tau_{xx(i,j)} = 2\mu_{(i,j)}\left[\frac{u_{(i,j)} - u_{(i,j-1)}}{\Delta x}\right] - \frac{2}{3}\mu_{(i,j)}\left[\frac{u_{(i,j)} - u_{(i,j-1)}}{\Delta x} + \frac{v_{(i+1,j)} - v_{(i-1,j)}}{2\Delta y}\right]$$

$$\tau_{xy} = \mu_{(i,j)}\left[\frac{u_{(i+1,j)} - u_{(i-1,j)}}{2\Delta y} + \frac{v_{(i,j)} - v_{(i,j-1)}}{\Delta x}\right]$$

25

$$q_x = -k_{(i,j)} \frac{T_{(i,j)} - T_{(i,j-1)}}{\Delta x}$$

and those in **F** are discretized as follows:

$$\tau_{yy(i,j)} = 2\mu_{(i,j)} \left[\frac{v_{(i,j)} - v_{(i-1,j)}}{\Delta x} \right] - \frac{2}{3}\mu_{(i,j)} \left[\frac{u_{(i,j+1)} - u_{(i,j-1)}}{2\Delta x} + \frac{v_{(i,j)} - v_{(i-1,j)}}{\Delta y} \right]$$

$$\tau_{xy} = \mu_{(i,j)} \left[\frac{u_{(i,j)} - u_{(i-1,j)}}{\Delta y} + \frac{v_{(i,j+1)} - v_{(i,j-1)}}{2\Delta x} \right]$$

$$q_y = -k_{(i,j)} \frac{T_{(i,j)} - T_{(i-1,j)}}{\Delta y}$$

while for corrector step terms appearing in **E** as follows:

$$\tau_{xx(i,j)} = 2\mu_{(i,j)} \left[\frac{u_{(i,j+1)} - u_{(i,j)}}{\Delta x} \right] - \frac{2}{3}\mu_{(i,j)} \left[\frac{u_{(i,j+1)} - u_{(i,j)}}{\Delta x} + \frac{v_{(i+1,j)} - v_{(i-1,j)}}{2\Delta y} \right]$$

$$\tau_{xy} = \mu_{(i,j)} \left[\frac{u_{(i+1,j)} - u_{(i-1,j)}}{2\Delta y} + \frac{v_{(i,j+1)} - v_{(i,j)}}{\Delta x} \right]$$

$$q_x = -k_{(i,j)} \frac{T_{(i,j)} - T_{(i,j-1)}}{\Delta x}$$

and those appearing in **F** are discretized as follows:

$$\tau_{yy(i,j)} = 2\mu_{(i,j)} \left[\frac{v_{(i+1,j)} - v_{(i,j)}}{\Delta y} \right] - \frac{2}{3}\mu_{(i,j)} \left[\frac{u_{(i,j+1)} - u_{(i,j-1)}}{2\Delta x} + \frac{v_{(i+1,j)} - v_{(i,j)}}{\Delta y} \right]$$

$$\tau_{xy} = \mu_{(i,j)} \left[\frac{u_{(i+1,j)} - u_{(i,j)}}{\Delta y} + \frac{v_{(i,j+1)} - v_{(i,j-1)}}{2\Delta x} \right]$$

$$q_y = -k_{(i,j)} \frac{T_{(i,j)} - T_{(i-1,j)}}{\Delta y}$$

After each predictor or corrector step, the physical variables are obtained by decoding the vector **U**;

$$\rho_{i,j} = \mathbf{U}_1$$
$$u_{i,j} = \frac{\mathbf{U}_2}{\mathbf{U}_1}$$
$$v_{i,j} = \frac{\mathbf{U}_3}{\mathbf{U}_1}$$
$$\mathbf{E}_{t_{i,j}} = \mathbf{U}_4$$
$$e_{i,j} = \frac{\mathbf{U}_4}{\mathbf{U}_1} - \frac{u_{i,j}^2 + v_{i,j}^2}{2}$$

$$(3.7)$$

with $\rho_{i,j}, u_{i,j}, v_{i,j}$ and $e_{i,j}$ obtained, the remaining flow-field properties are determined by using the following relations:

$$T_{i,j} = \frac{e_{i,j}}{c_v}$$
$$p_{i,j} = \rho_{i,j} R T_{i,j}$$
$$\mu_{i,j} = \mu_0 \left(\frac{T_{i,j}}{T_0}\right)^{\frac{3}{2}} \frac{T_0 + 110}{T_{i,j} + 110}$$
$$k_{i,j} = \frac{\mu_{i,j} c_p}{Pr}$$

$$(3.8)$$

where Pr is the Prandtl number taken to be constant at 0.71.

3.4 Discretization of Boundary Conditions

The y derivatives on the inflow boundary are obtained by forward difference while that on outflow boundary is determined by backward difference. On the other hand the x derivatives on the plate surface is determined by forward difference and that

on the upper boundary is obtained by backward difference. e.g. for plate surface and upper boundary

$$\left(\frac{\partial u}{\partial y}\right)_{(i,j)} = \frac{u_{(2,j)} - u_{(1,j)}}{\Delta y}$$

$$\left(\frac{\partial u}{\partial y}\right)_{(IMAX,j)} = \frac{u_{(IMAX,j)} - u_{(IMAX-1,j)}}{\Delta y}$$

and for inflow and outflow boundary

$$\left(\frac{\partial u}{\partial x}\right)_{(i,1)} = \frac{u_{(i,2)} - u_{(i,1)}}{\Delta x}$$

$$\left(\frac{\partial u}{\partial x}\right)_{(i,JMAX-1)} = \frac{u_{(i,JMAX)} - u_{(i,JMAX)}}{\Delta x}$$

3.5   Calculation of Time-Step

For the calculation of size of the time-step, the Courant-Friedrichs-Lewy (CFL) criterion is used [40]. $a_{i,j}$ is the local speed of sound in metres per second and K_f is the Courant number. K_f acts as a "fudge factor", to make the solution stable.

$$(\Delta t_{CFL})_{i,j} = \left[\frac{|u_{i,j}|}{\Delta x} + \frac{|v_{i,j}|}{\Delta y} + a_{i,j}\sqrt{\frac{1}{\Delta x^2} + \frac{1}{\Delta y^2}} + 2v'\left(\frac{1}{\Delta x^2} + \frac{1}{\Delta y^2}\right)\right]^{-1} \quad (3.9)$$

where

$$v' = \max\left[\frac{\frac{4}{3}\mu_{i,j}\left(\gamma\mu_{i,j}/Pr\right)}{\rho_{i,j}}\right] \quad (3.10)$$

Now time step

$$\Delta t = \min\left[K_f\left(\Delta t_{CFL}\right)_{i,j}\right] \quad (3.11)$$

for $0.5 \leq K_f \leq 0.8$

3.6   Solution Procedure

As initial estimates, values are assigned to initialize the variables. MacCormack scheme is then applied to find the values of the variables at the next time step. Boundary condition is applied at the boundary points. Values at the next time is obtained

28

until the difference in density at any point in present time and that at the same point in the next time step is of the order of 10^{-8} kg/m^3.

Shear stress and heat transfer on the plate surface are obtained by forward difference. The solution procedure can be summarized as follows:

1. Initiialize the variables u,v,p,T at all the grid points.

2. Find other variables ρ, E, e, μ, k using present value of u, v, p and T.

3. Calculate the time step by the CFL criterion.

4. Find the values of the variables in the next time step by MacCormack scheme.

5. Apply boundary conditions.

6. Check the convergence, if convergence condition is met go to Step 7. Otherwise go back to Step 2.

7. Calculate skin friction and heat transfer on the surface.

Chapter 4

Results and Discussion

The numerical procedure given in the preceding chapter is implemented successfully for the Mach numbers 4, 8 and 12 over a flat plate and wedge at various angles. The computer system used for this purpose is HP-9000 of IIT Kanpur computer centre. On a pentium-II processor with 64 MB RAM the program needs 55 KB RAM and at 100% CPU the program converges in 25 minutes. The disk space available to run the program is 20 MB. The results obtained are for surface length of 0.00001 m. and other properties are equal to those of standard sea level. The results obtained in this thesis for the hypersonic viscous flow regime are validated using results obtained in Ref.[40].

4.1 Validation of the Code

The validity of the code developed is shown by obtaining the results of Mach number 4 for 70X70 grid and comparing them with the results obtained in Ref. [40]. These comparison plots are given in Fig.(4.1). The results obtained for comparison are pressure, temperature and velocity profile, Mach number at the outflow boundary and normailized pressure distribution on the surface of the plate. The normalized y

distance (y_n) has been obtained from

$$y_n = \frac{y}{x}\sqrt{Re_x}$$

where $Re_x = \frac{\rho_e u_e x}{\mu_e}$

4.2   Results for Flat Plate

The plots shown in Fig. (4.2), (4.3) and (4.4) are of normalized pressure, velocity and temperature profiles, surface pressure distribution, skin friction coefficient and rate of heat transfer for various number of grid points (20X20, 50X50, 70X70 and 90X90) in the computational domain at Mach numbers 4, 8 and 12 respectively. Plots (A), (B) and (C) in all the three figures show that pressure, temperature and velocity profiles are approximately the same for grid 70X70 and 90X90, but plots (D), (E) and (F) show that normalized pressure, skin friction coefficient and rate of heat transfer on the plate surface at grid 70X70 and 90X90 are quite different. This observation shows that more accurate results can be obtained by taking finer grids near the surface.

Fig. (4.5) shows that for Mach number 8 results, from 90X90 uniform and 40X40 non-uniform grids are nearly the same, while they are very much different for Mach 4 and 12. This shows that non-uniformity distribution of grids should be a function of Mach number.

Plots shown in Fig. (4.6) are of normalized pressure and temperature profiles obtained at various times for Mach numbers 4, 8 and 12. These plots reveal that in shock capturing technique shock develops at any location with time instead of moving from one location to other. Pressure, temperature and velocity profiles obtained in plots A, B and C of Fig. (4.7) show reduction in shock layer thickness and increase in strength of the shock with increase in Mach number. Plots D and F show increase in pressure and heat transfer while plot E shows reduction in skin friction coefficient with Mach numbers. This reduction of skin friction coefficient does not mean that

frictional force reduces with Mach number, actually the (V_∞^2) term in relation

$$c_f = \frac{\tau_{xy}}{\frac{1}{2}\rho_\infty V_\infty^2} \tag{4.1}$$

reduces c_f with Mach number.

From Fig. (4.8) it is observed that $c_f\sqrt{Re_x}$ and $c_H\sqrt{Re_x}$ calculated from full Navier-Stokes equations are less than those calculated from boundary-layer equations. The reason for this is that the density of the flow at the boundary layer increases due to shock. Also it goes on increasing rapidly with Mach number. It is clear from these expressions

$$c_f\sqrt{Re_x} = \frac{\tau_{xy}}{\frac{1}{2}\rho_e u_e^2}\sqrt{\frac{\rho_e u_e x}{\mu_e}} \tag{4.2}$$

$$c_H\sqrt{Re_x} = \frac{q_w}{\rho_e u_e c_p \left(T_e + r\frac{u_e^2}{2T} - T_w\right)}\sqrt{\frac{\rho_e u_e x}{\mu_e}} \tag{4.3}$$

that the term $\sqrt{\rho_e}$ at the denominator increases with Mach number and hence decreases the value of the term on the left hand side of the Equations (4.2) and (4,3).

4.3   Results for Wedges

Plot (A) in Fig (4.9) shows coefficient of pressure distribution on a wedge surface for various Mach numbers. It is evident from the plot that as the Mach number increases, the coefficient of pressure decreases and comes closer to Newtonian pressure distribution. This reduction of coefficient of pressure does not mean that the actual pressure on the wall decreases with Mach number M_{infty}. It is clear from the expression

$$c_p = \frac{p - p_\infty}{\frac{1}{2}\rho_\infty V_\infty^2} = \frac{p - p_\infty}{\frac{1}{2}\gamma p_\infty M_\infty^2} \tag{4.4}$$

that although c_p decreases gradually with Mach number, pressure on the surface increases considerably as Mach number increases due to the M_∞^2 variation. Plot (B) shows increase in pressure coefficient with wedge angle. It is also evident from plot (B) that deviation from Newtonian pressure distribution increases with Wedge angle.

Fig. (4.10) shows reduction in skin friction coefficient and increase in rate of heat transfer with Mach number for a wedge of wedge angle 10 degrees. Fig. (4.11) shows reduction in shock layer thickness and increase in it's strength with Mach number for a Wedge at angle 10 degrees. Fig. (4.12), (4.13) and (4.14) show comparision of pressure, temperature and velocity profiles at the outflow boundary for a wedge at angle 10 degrees with those for a flat plate at Mach numbers 4, 8 and 12 respectively. The comperision of these plots with one another show that the rate of increase in shock strength and reduction in shock layer thickness with Mach number for a wedge is higher than those for a flat plate.
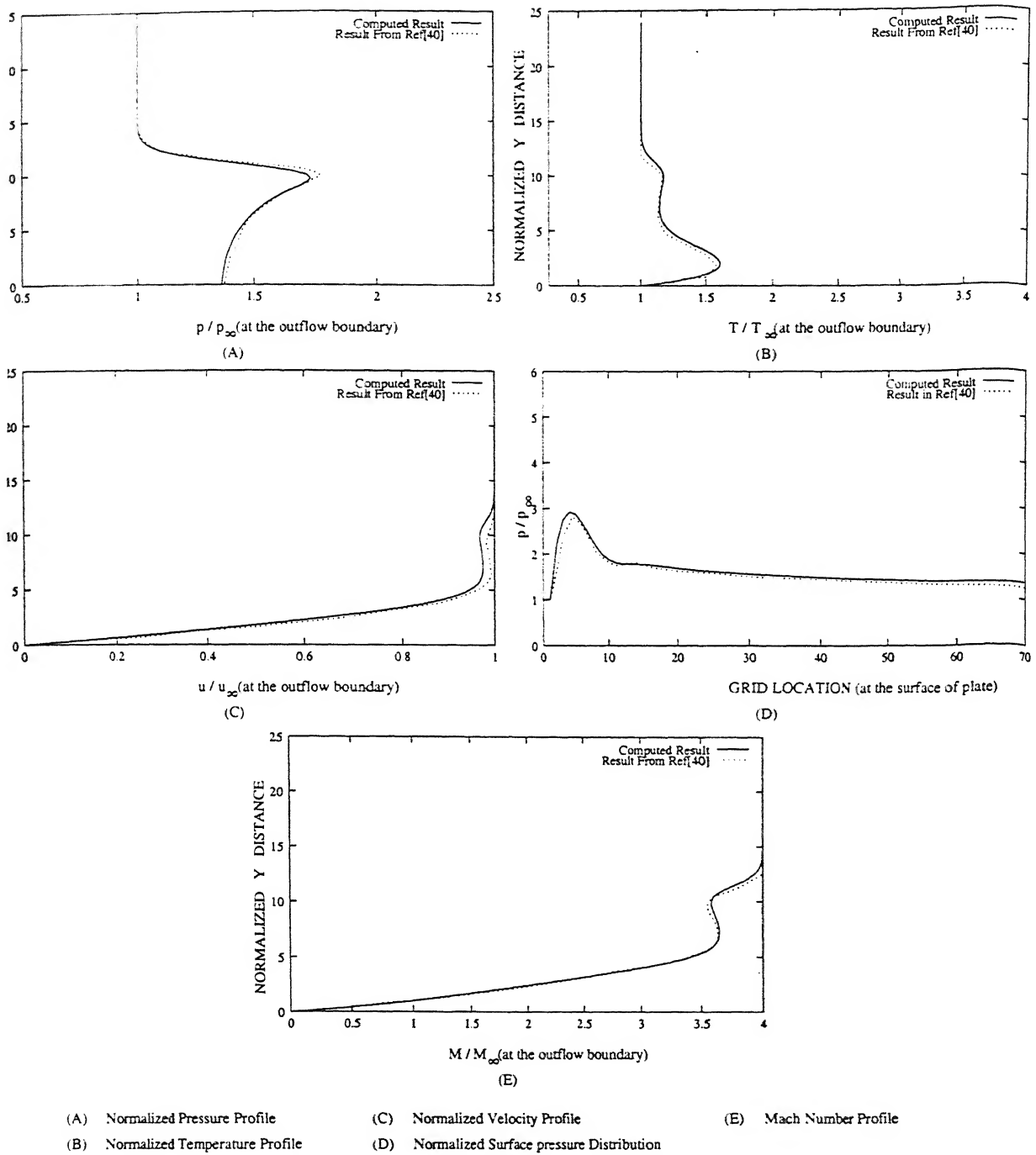
Figure 4.1: Comparison Between Computed Results and Results Given in Ref. [40]

34

(A) Normalized pressure profile   (C) Normalized velocity profile   (E) Skin Friction Coefficient on Surface of Plate

(B) Normalized temperature profile   (D) Normalized surface pressure distribution   (F) Rate of Heat Transfer on Surface of Plate
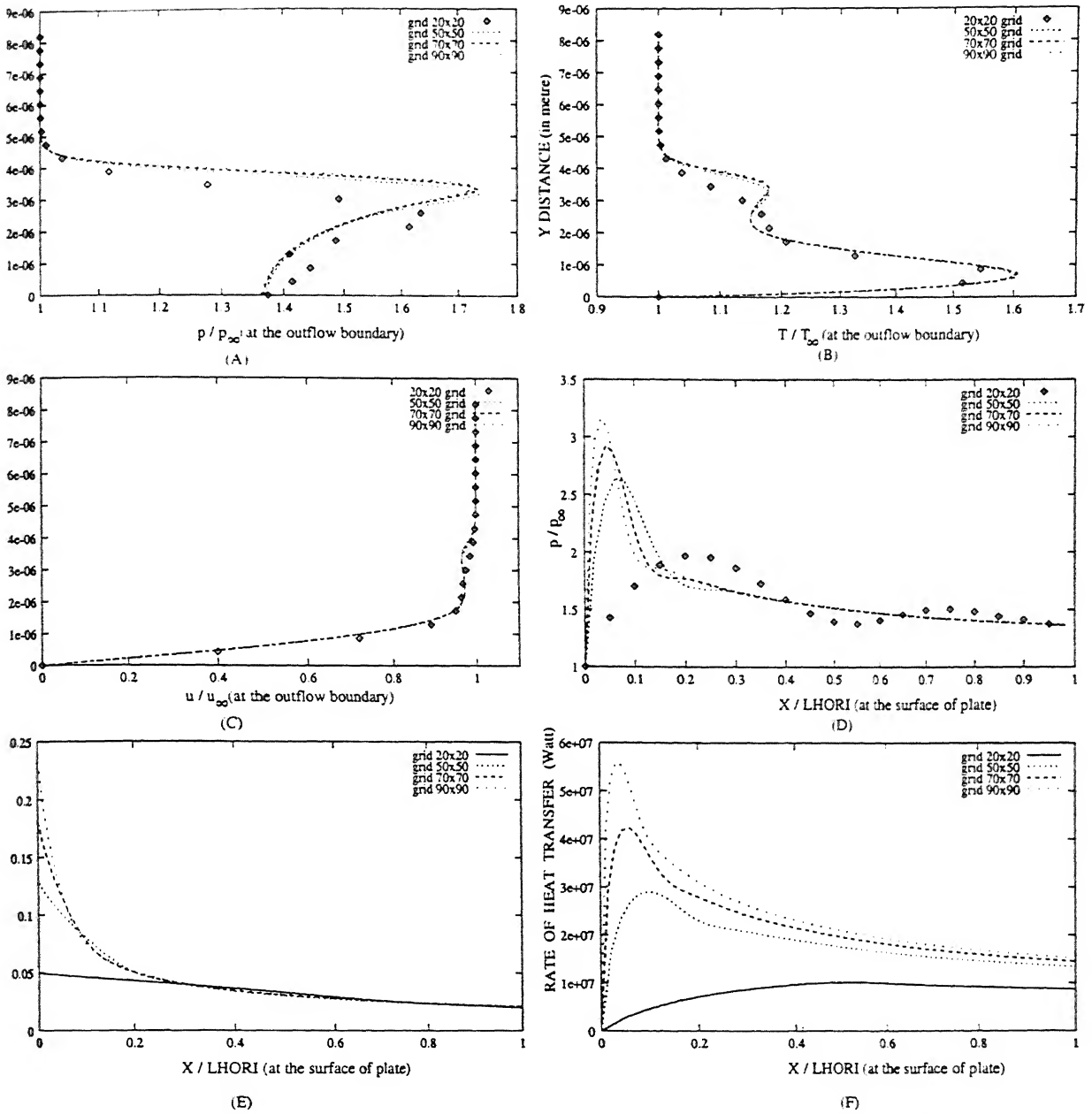
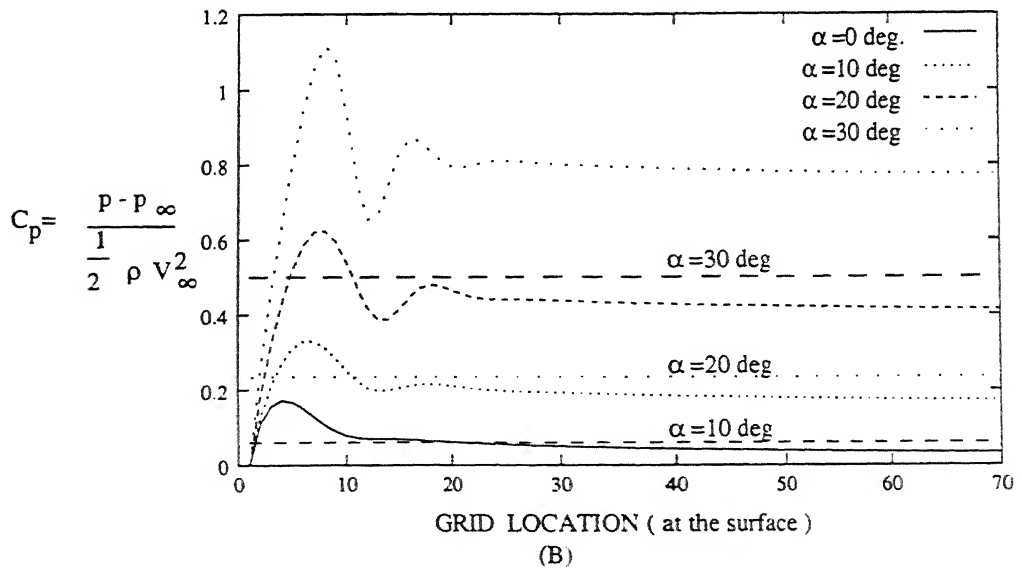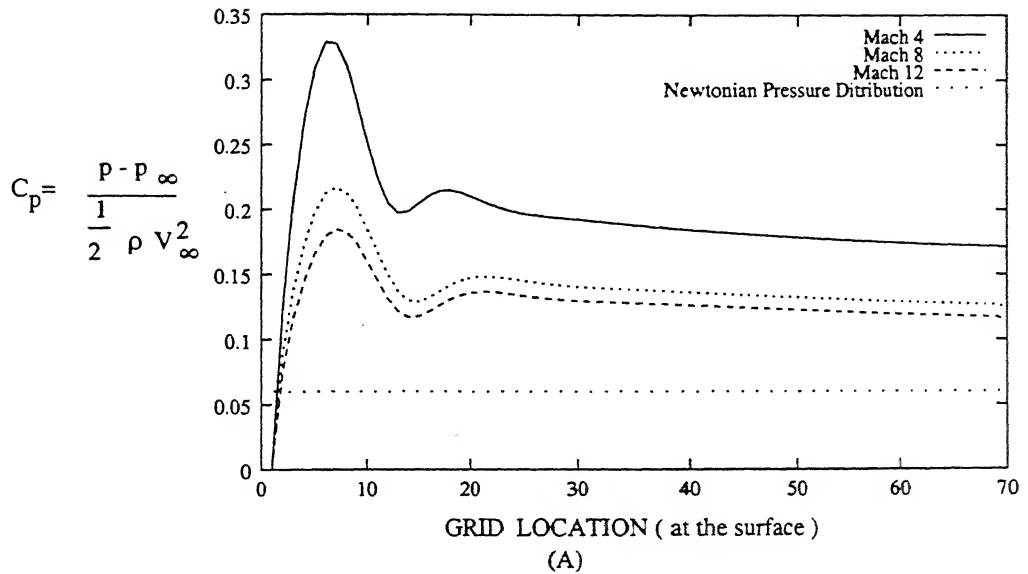Figure 4.2: Comparison of Various Parameters for Different Number of Grid Points Mach Number 4 and Sea-Level Condition
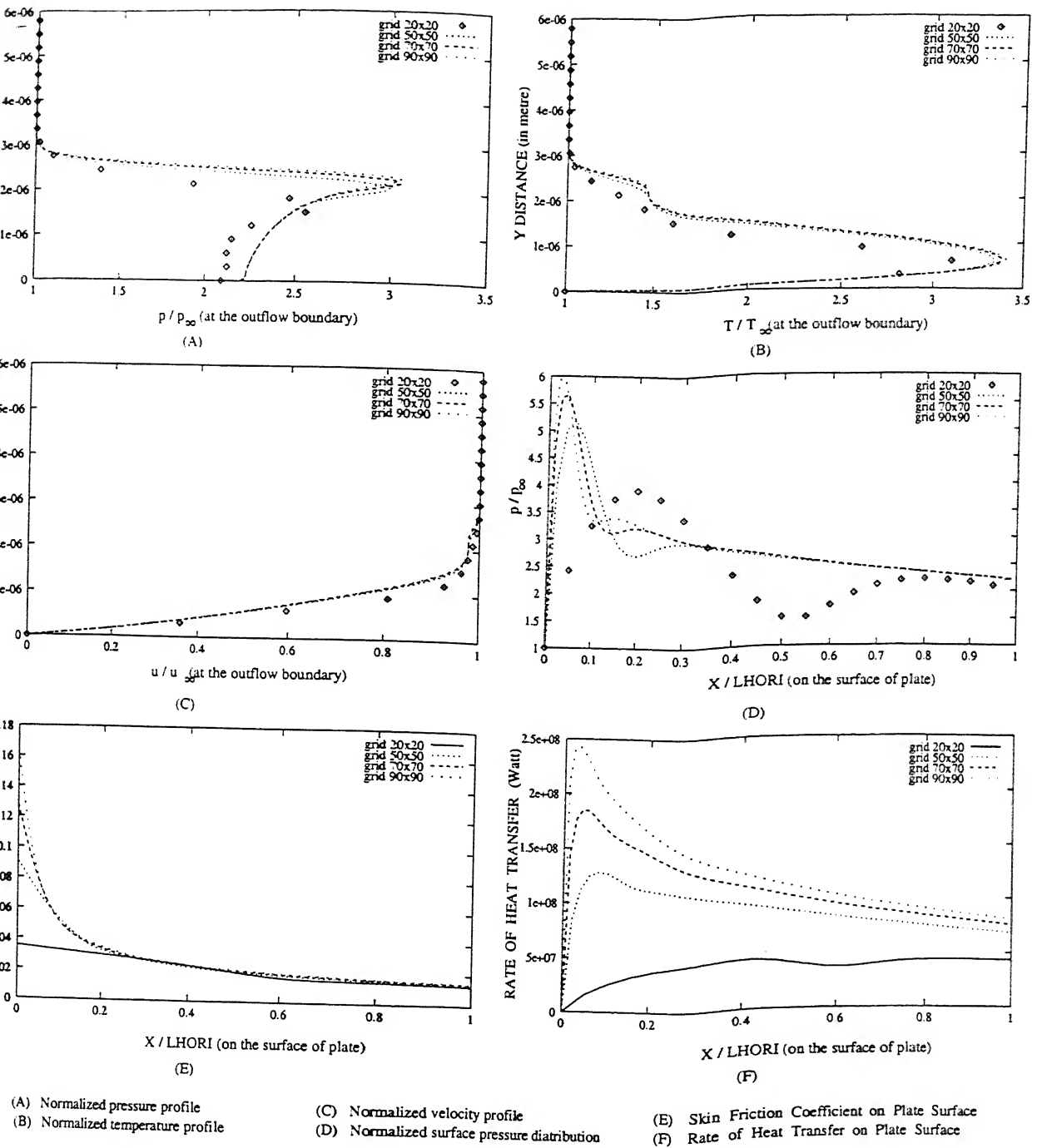
Figure 4.3: Comparison of Various Parameters for Different Number of Grid Points
Mach Number 8 and Sea-Level Condition

36
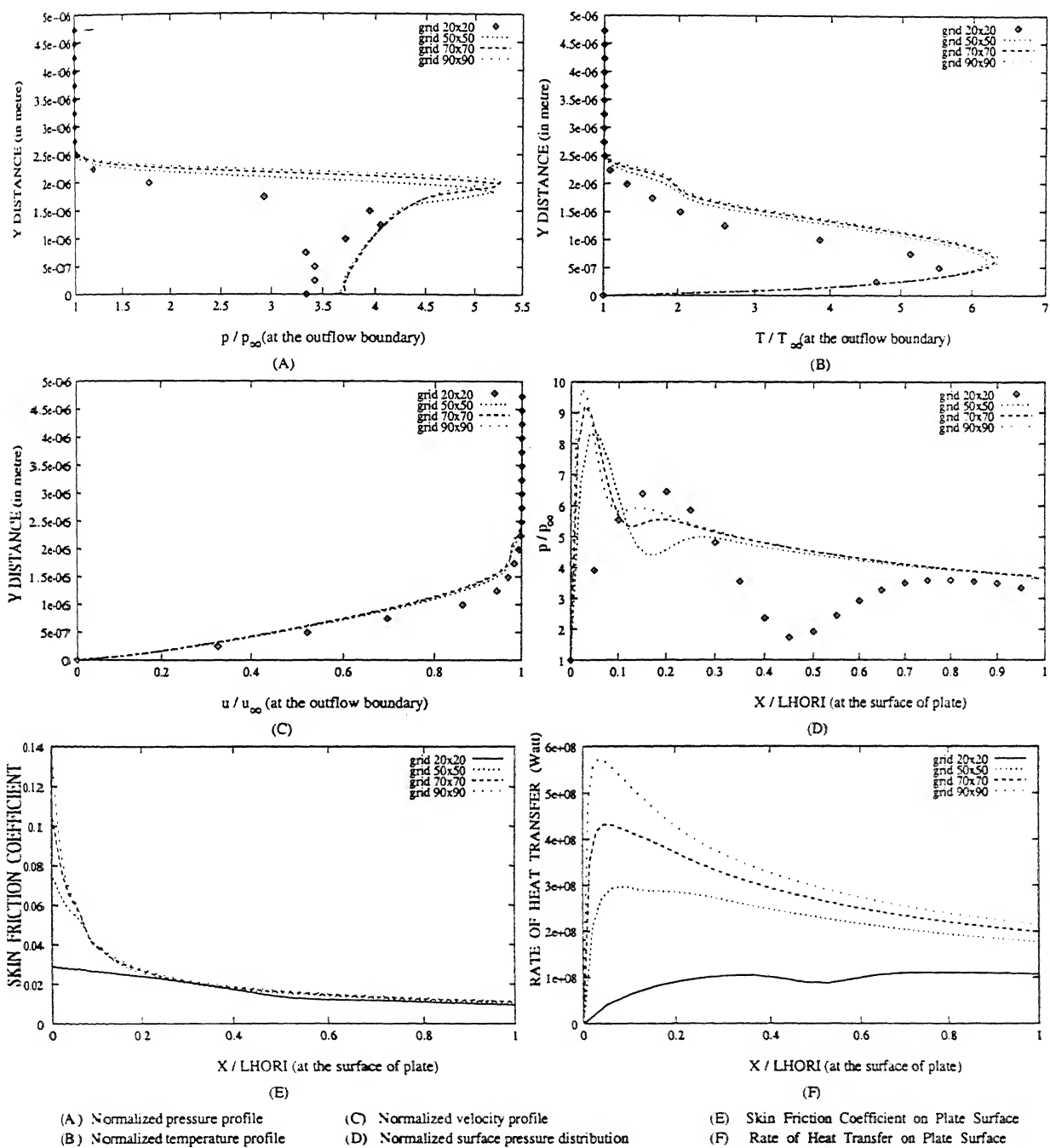
Figure 4.4: Comparison of Various Parameters for Different Number of Grid Points at Mach Number 12 and Sea-Level Condition
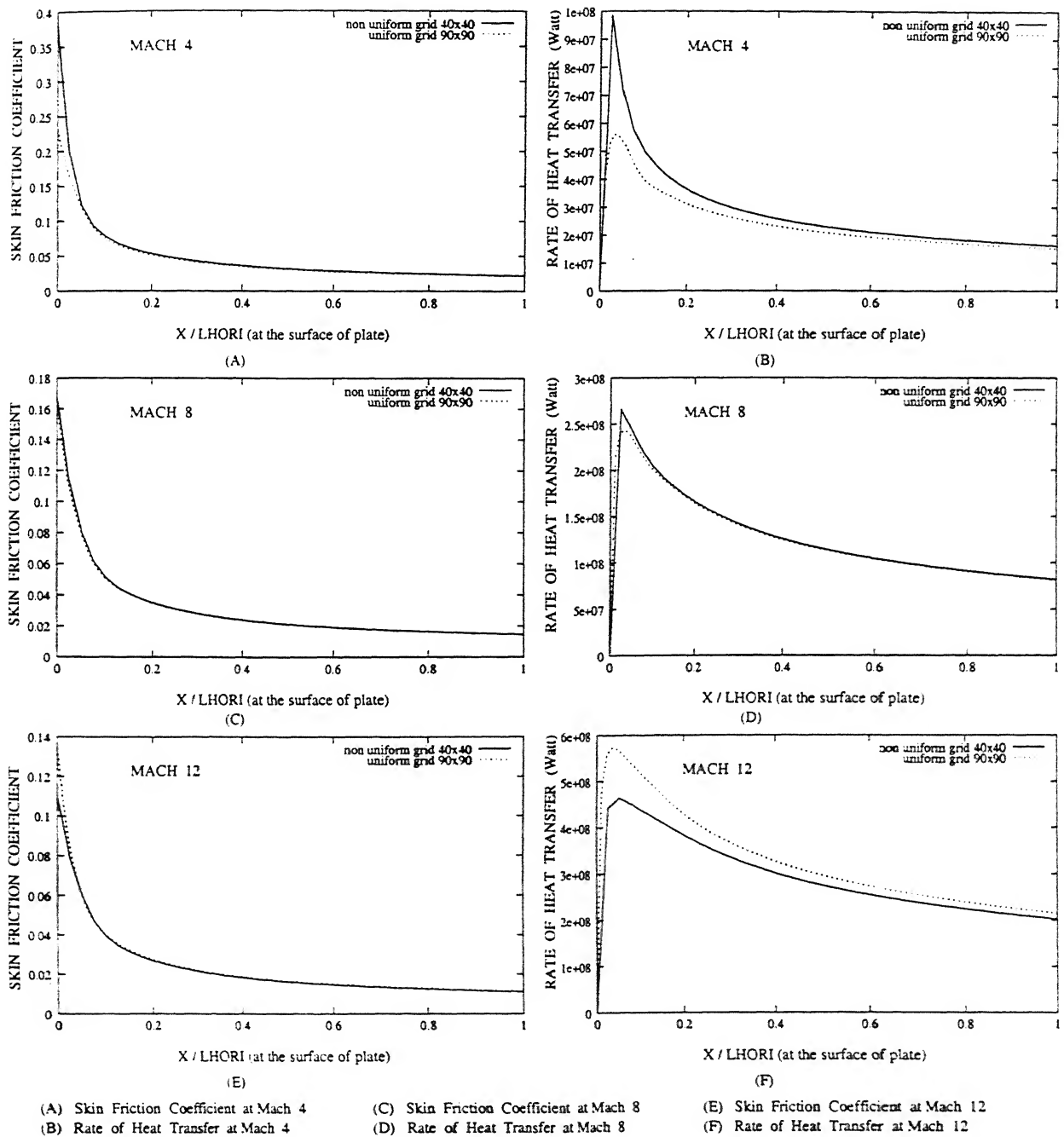
Figure 4.5: Comparison of Skin Friction and Rate of Heat Transfer on the Plate Surface for Uniform and Non-Uniform Grids at Different Mach Numbers
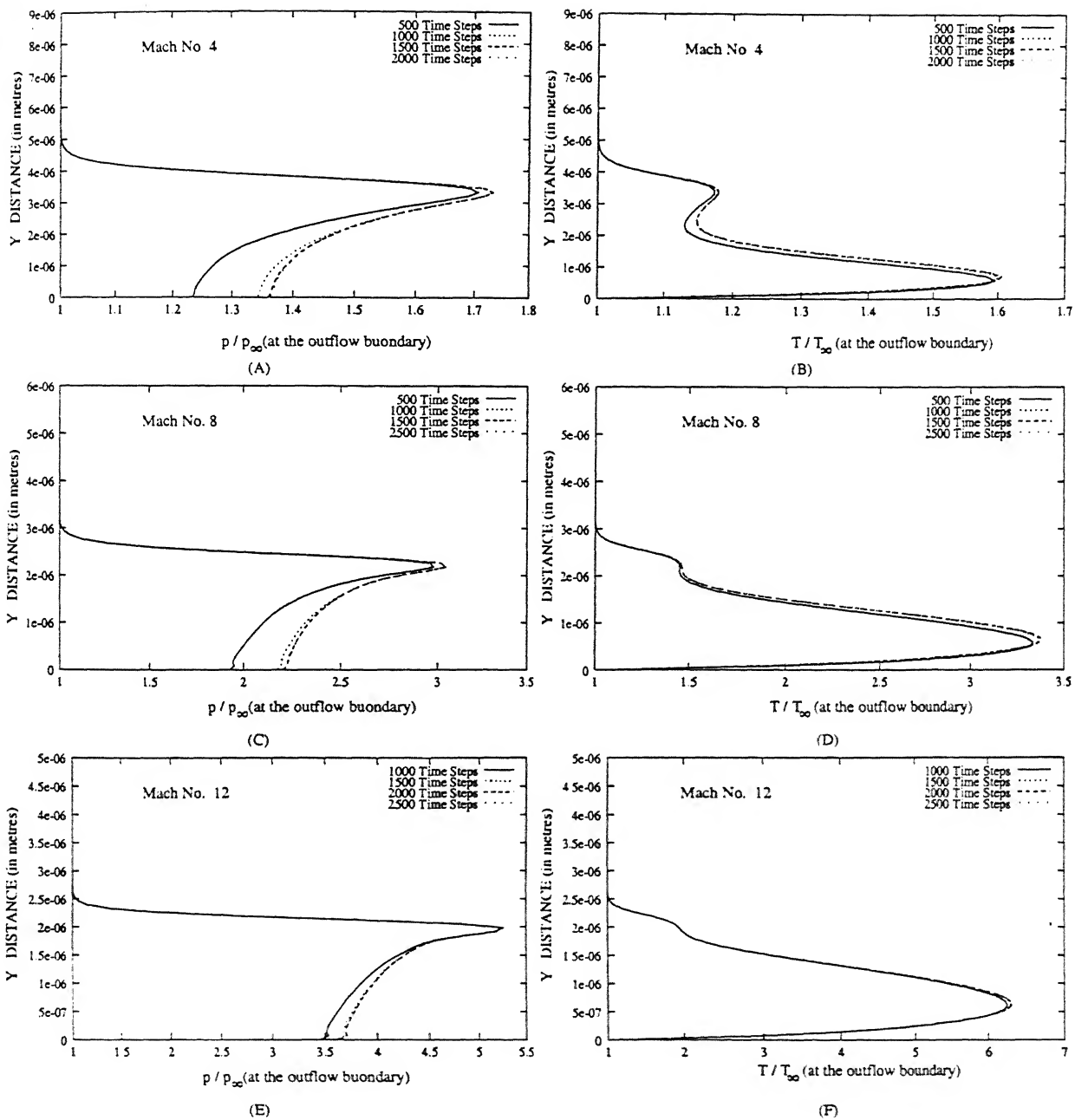
(A) Normalized Pressure Profiles at Mach 4   (C) Normalized Pressure Profiles at Mach 8   (E) Normalized Pressure Profiles at Mach 12
(B) Normalized Temperature Profiles ai Mach 4   (D) Normalized Temperature Profiles ai Mach 8   (F) Normalized Temperature Profiles at Mach 12

Figure 4.6: Representation of Normalized Pressure and Temperature Profiles at Various Time Steps for Different Mach Numbers and 70×70 Grid

Figure 4.7: Comparison of Various Parameters for Different Mach Numbers

Flat Plate Skin Friction Coefficients

Flat Plate Stanton Numbers
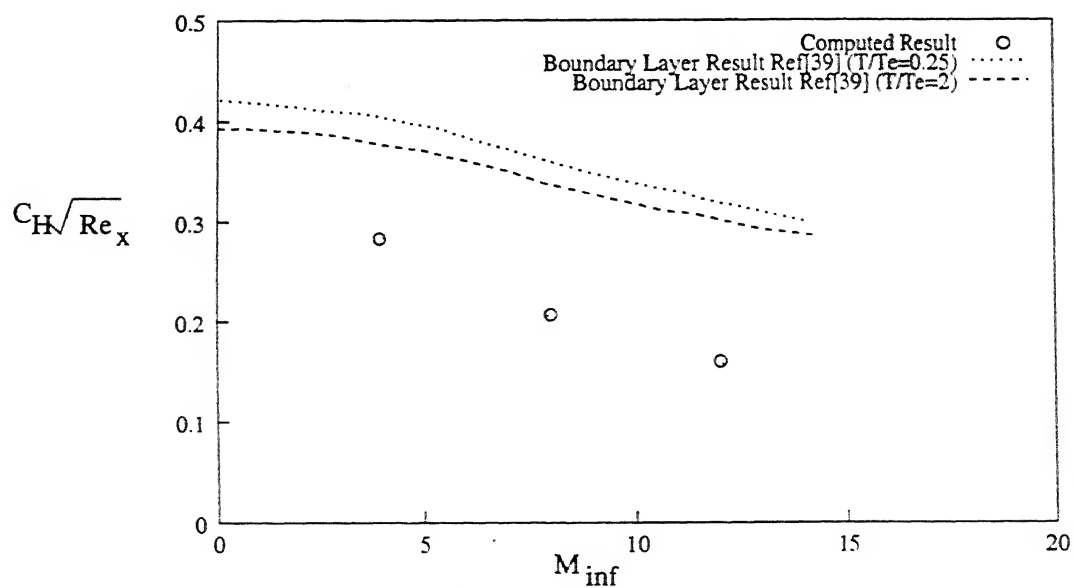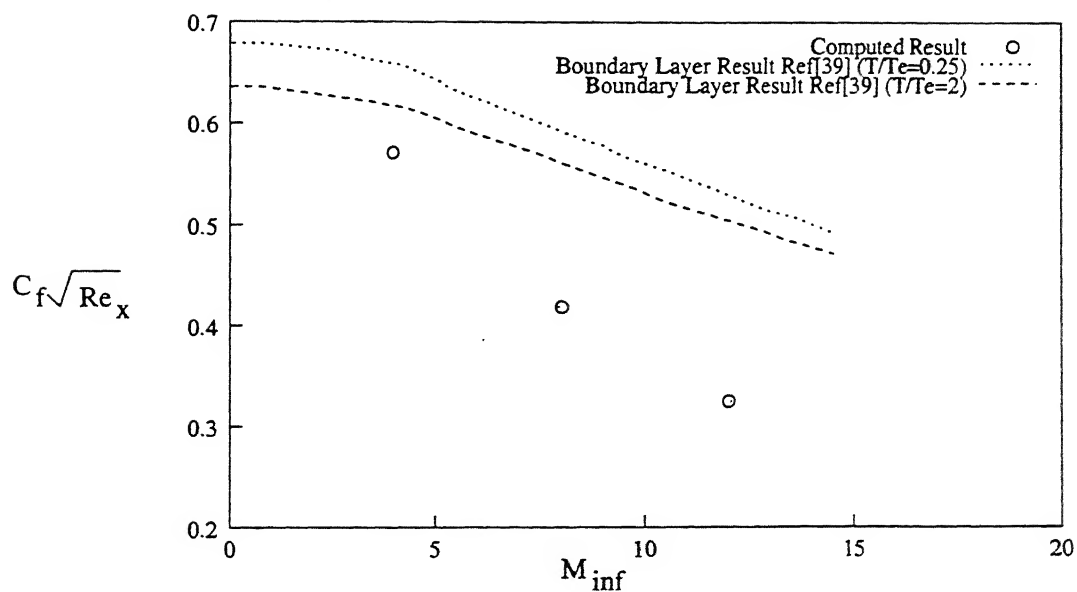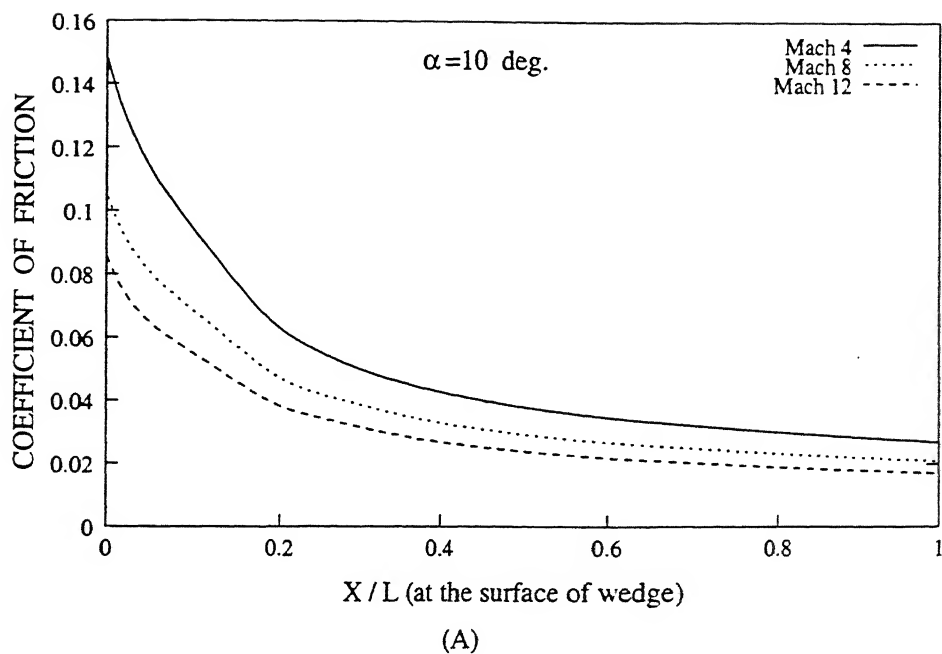
Figure 4.8: Comparison of Skin Friction Coefficients and Stanton Numbers for Boundary Layers and Computed Results

$$C_p = \frac{p - p_\infty}{\frac{1}{2} \rho V_\infty^2}$$

GRID LOCATION (at the surface)

(A)

$$C_p = \frac{p - p_\infty}{\frac{1}{2} \rho V_\infty^2}$$

GRID LOCATION (at the surface)

(B)

(A)   Comparision of Coefficient of Pressure for Various Mach Numbers

(B)   Comparision of Coefficient of Pressure for Various Wedge Angles
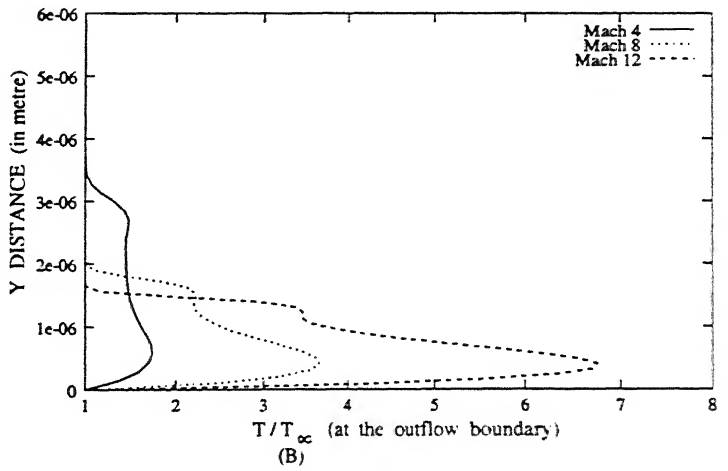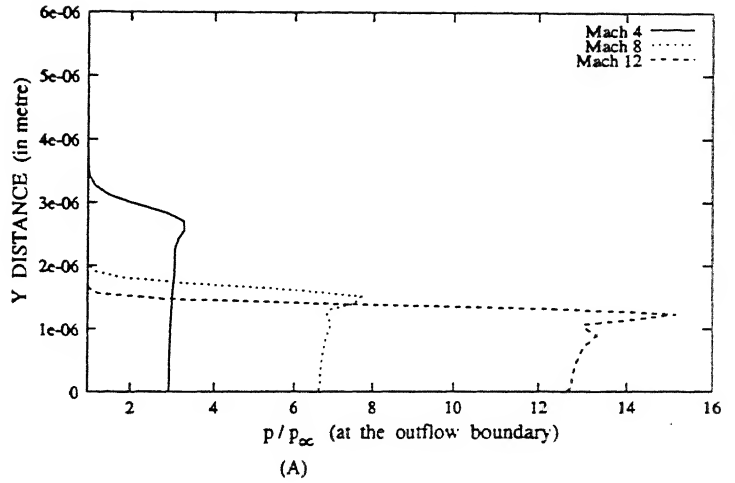(straight lines are Newtonian approximation at given angle)

Figure 4.9: Comparison Plots of Wedge
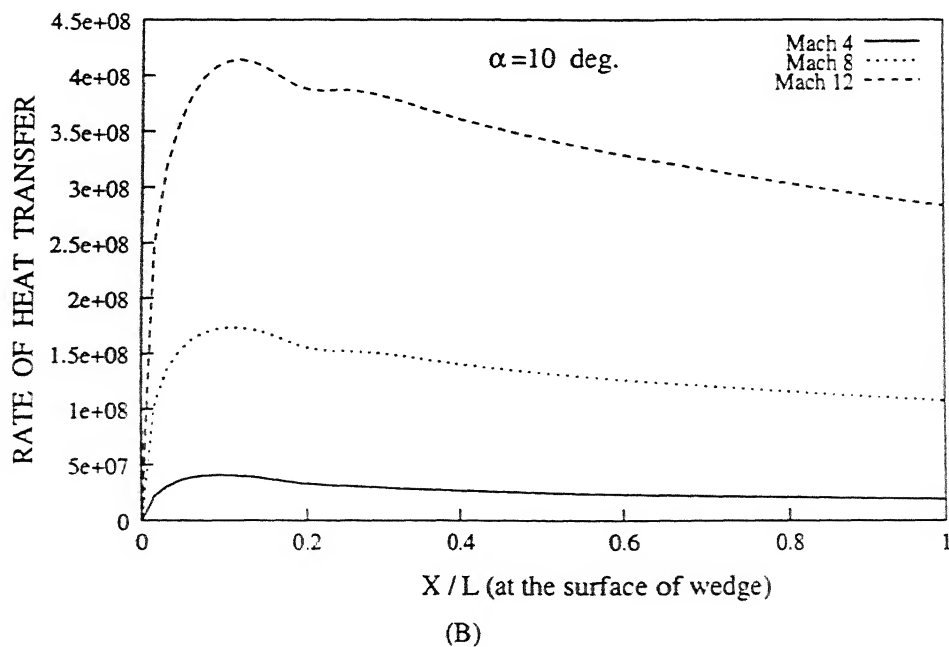
(A) Coefficient of friction for various Mach numbers
(B) Rate of heat transfer for various Mach numbers

Figure 4.10: Comparison of Coefficient of Friction and Rate of Heat Transfer for Various Mach Numbers for a Wedge at Grid 70×70
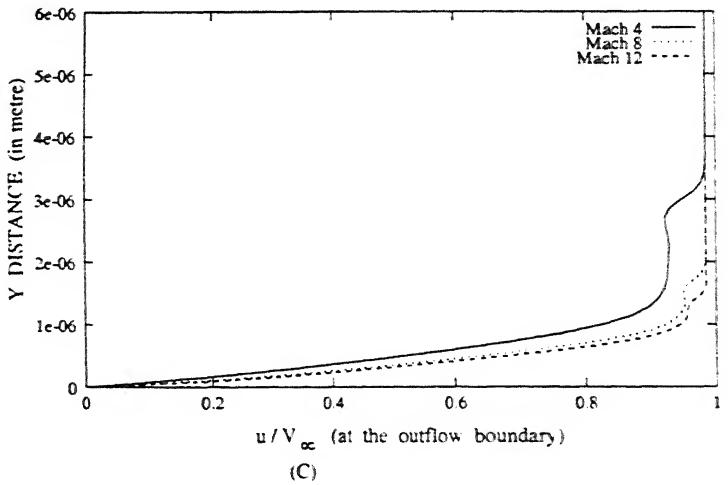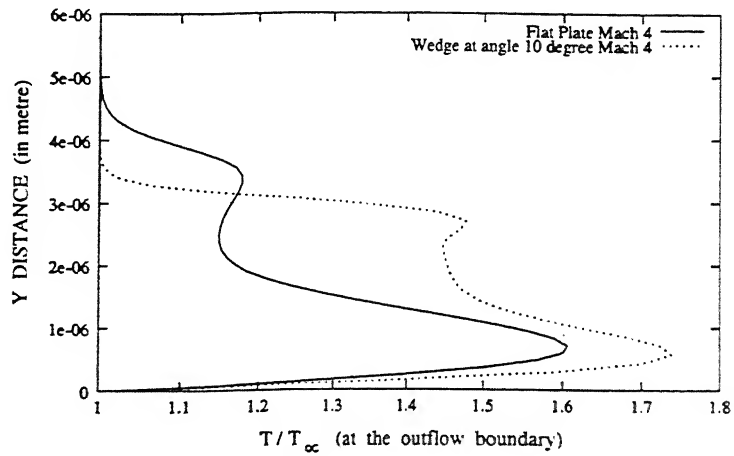
(A) Normalized pressure profile

(B) Normalized temperature profile
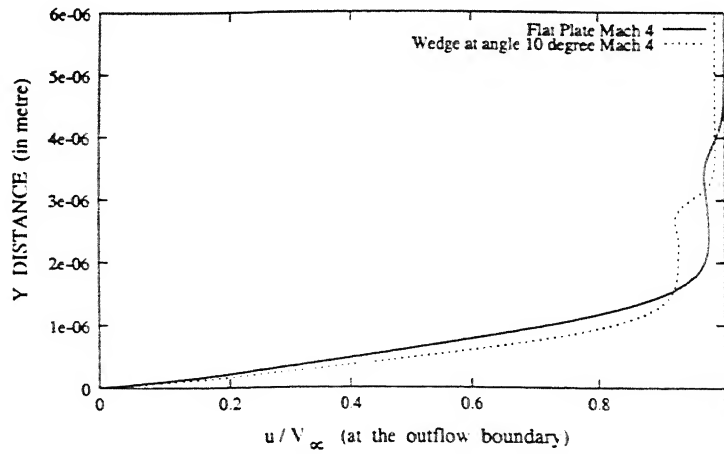
(C) Normalized velocity profile

Figure 4.11: Comparison of Pressure, Temperature and Velocity Profiles at Various Mach Numbers for Wedge of Angle 10 Degrees and Grid 70×70
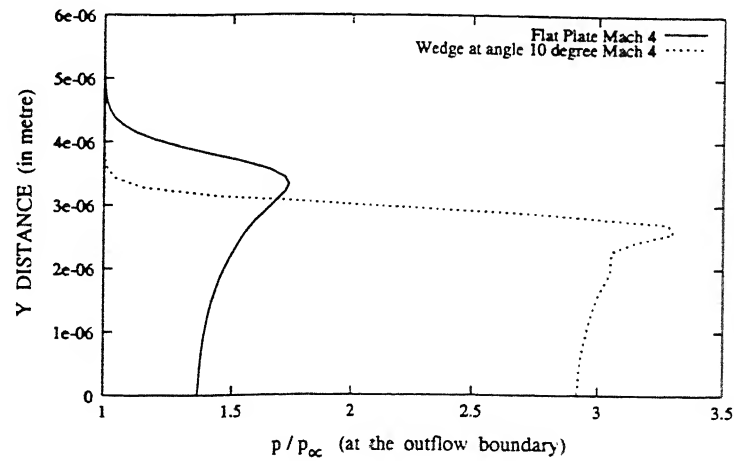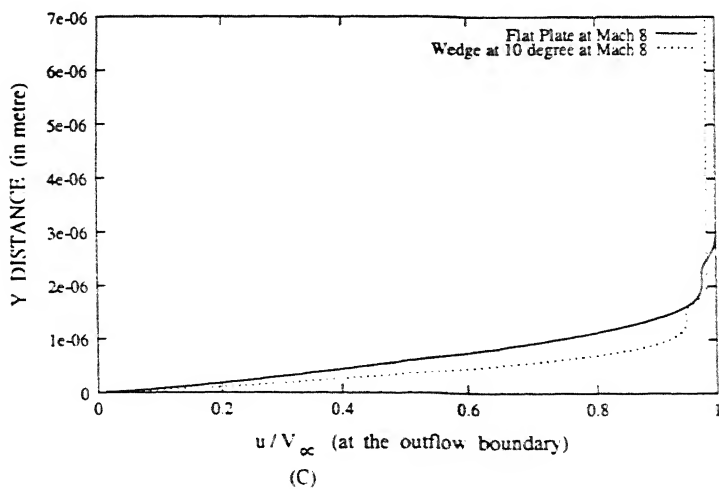
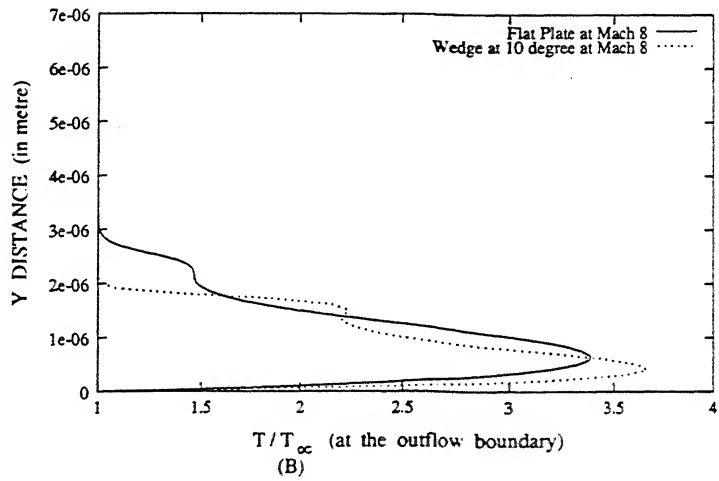(A) Normalized pressure profile

(B) Normalized temperature profile

(C) Normalized velocity profile

Figure 4.12: Comparison of Pressure, Temperature and Velocity Profiles for Flat Plate and Wedge of Angle 10 Degrees at Mach Number 4 and Grid 70×70

(A) Normalized pressure profile

(B) Normalized temperature profile

(C) Normalized velocity profile

Figure 4.13: Comparison of Pressure, Temperature and Velocity Profiles for Flat Plate and Wedge of Angle 10 Degrees at Mach Number 8 and Grid 70×70
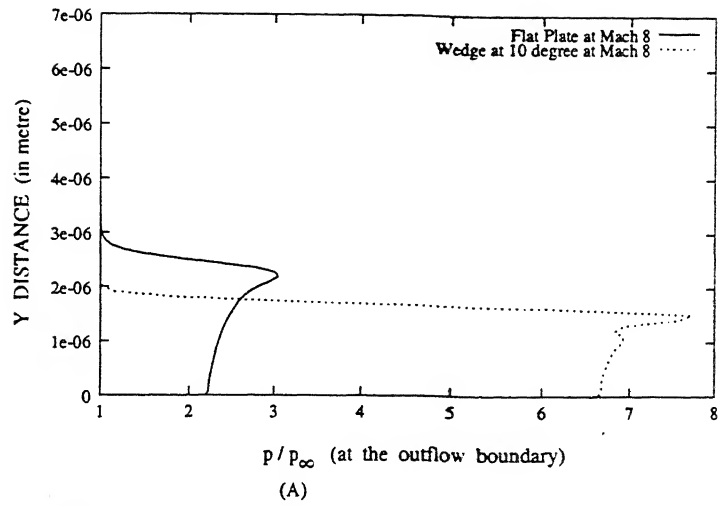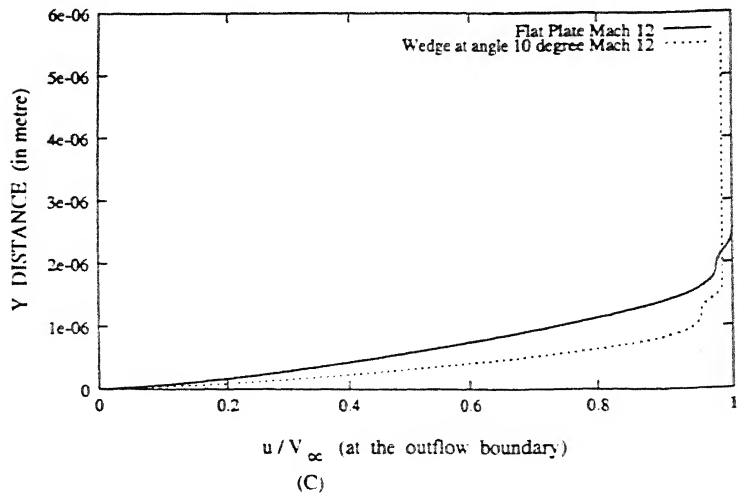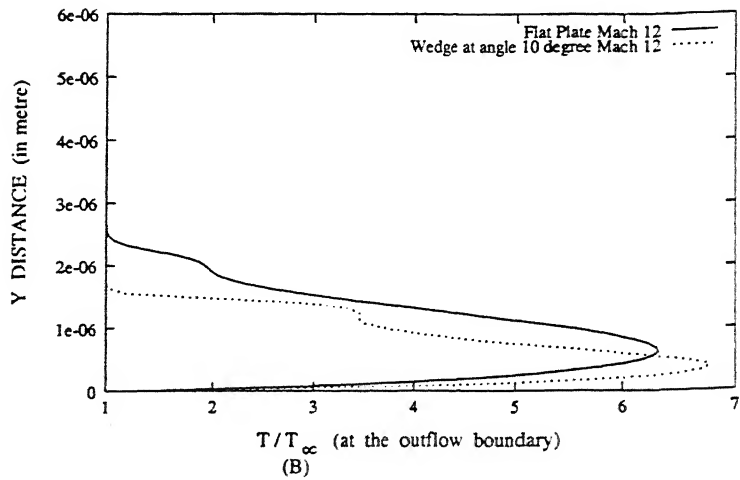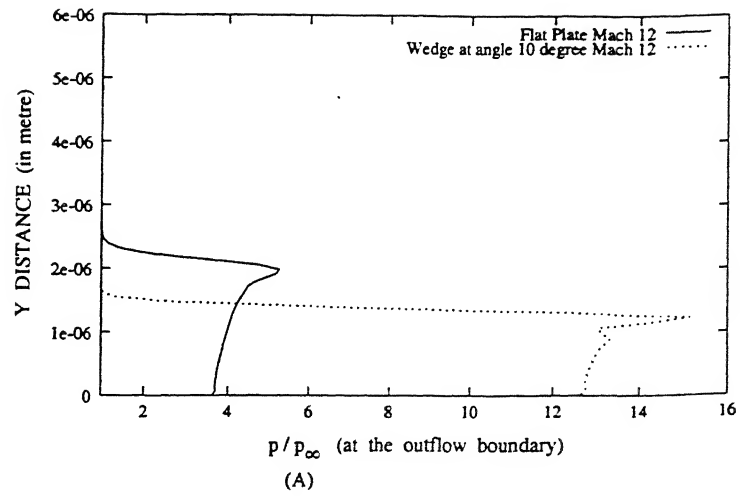
(A) Normalized pressure profile

(B) Normalized temperature profile

(C) Normalized velocity profile

Figure 4.14: Comparison of Pressure, Temperature and Velocity Profiles for Flat Plate and Wedge of Angle 10 Degrees at Mach Number 12 and Grid 70×70

Chapter 5

Conclusions and Suggestions for Future Work

5.1 Conclusions

In this work the hypersonic viscous flow over a flat plate and wedges has been studied numerically, by the solution of Navier-Stokes equations using time marching finite difference method and shock capturing technique. These in turn have been further processed numerically to estimate the values of the individual skin friction coefficient and rates of heat transfer for various Mach numbers.

Results show that increase in number of grid point in the domain increases the accuracy of the results. As expected, results of same and even higher accuracy have been obtained with less number of grid points when grids are nonuniform with higher density nearer to the surface of the plate. The distribution of nonuniformity for certain order of accuracy is found to be a function of Mach number.

Increase in intensity of shock layer and decrease in thickness of the shock layer with Mach number is obtained as per expectation. Results after various time steps show

the development of shock and gradual increase in coefficient and rate of heat transfer with time. It has been shown that skin friction coefficient and Stanton number for full Navier- Stokes equations are significantly less than those obtained by solving the boundary-layer equations.

Results obtained for wedge show the increase in skin friction coefficient and rate of heat transfer with increase in wedge angle.

5.2   Future Scope of the Work

Considerable scope exists for extending this work. The code can be used for the flow over a blunt-body by using a body-fitted grid and transforming it into a rectangular grid. It can also be made useful for an axisymmetric and three dimensional flow. For a three dimensional flow problem, the third spatial parameters of the Navier-Stokes equations are also considered.

The problem finds its important application in the analysis of effect of aerothermodynamics of the flow on the structural dynamics of the body. As observed at higher Mach numbers temperature and pressure on the body are very high. Since high temperature reduces the stiffness of the structure, both temperature and pressure at hypersonic speed causes large deflection on the body (wings of the aircraft).This interaction between aerothermodynamics and structural dynamics (called aerothermoelasticity) can cause strctural failure. Thus limit of the speed can exactly be defined by considering this effect. Chemical non-equilibrium effects can also be included in the code to make it accurate in the high Mach number range.

Appendix A

A.1 Forward Difference Scheme

Consider the Taylor series expansion of u_{i+1} around the point i.

$$u_{i+1} = u_i + \frac{\partial u}{\partial x}\Big|_i \frac{(x_{i+1} - x_i)}{1!} + \frac{\partial^2 u}{\partial x^2}\Big|_i \frac{(x_{i+1} - x_i)^2}{2!} + \cdots \tag{A.1}$$

If the distance between x_{i+1} and x_i is small, its square terms will be even smaller so that the second derivative and higher order terms can be neglected.

$$\frac{\partial u}{\partial x}\Big|_i = \frac{u_{i+1} - u_i}{x_{i+1} - x_i} \tag{A.2}$$

This is called forward difference of first derivative. In this approximation the order of accuracy is first.

For a regular grid, the distance between two consecutive points will be constant, i.e. $x_{i+1} - x_i = x_i - x_{i-1} = \Delta x$. Therefore the forward difference scheme of first derivative becomes

$$\frac{\partial u}{\partial x}\Big|_i = \frac{u_{i+1} - u_i}{\Delta x} \tag{A.3}$$

A.2 Backward Difference Scheme

Similarly, the forward difference involves expansion of u_{i-1} around i.

$$u_{i-1} = u_i - \frac{\partial u}{\partial x}\Big|_i \frac{(x_i - x_{i-1})}{1!} + \frac{\partial^2 u}{\partial x^2}\Big|_i \frac{(x_i - x_{i-1})^2}{2!} + \cdots \tag{A.4}$$

Again, if the distance between x_{i-1} and x_i is small, its square will be very small. So neglecting second order and higher order derivatives,

$$\frac{\partial u}{\partial x}\Big|_i = \frac{u_i - u_{i-1}}{x_i - x_{i-1}} \tag{A.5}$$

This is the so-called backward difference of first derivative which is accurate to within first order.

$$\frac{\partial u}{\partial x}\Big|_i = \frac{u_i - u_{i-1}}{\Delta x} \tag{A.6}$$

A.3 Central Difference Scheme

Subtracting (A.5) from (A.1) we will get

$$u_{i+1} - u_{i-1} = 2\frac{\partial u}{\partial x}\Big|_i \frac{(x_i - x_{i-1})}{1!} + 2\frac{\partial^3 u}{\partial x^3}\Big|_i \frac{(x_i - x_{i-1})^3}{3!} + \cdots \tag{A.7}$$

Neglect second order and higher order derivative terms, we can get

$$\frac{\partial u}{\partial x}\Big|_i = \frac{u_{i+1} - u_{i-1}}{x_{i+1} - x_{i-1}} \tag{A.8}$$

This is called the central difference of first derivative. Here the truncation of term is from third only. Therefore central difference approximation has accuracy of second order. For a regular grid, it will become

$$\frac{\partial u}{\partial x}\Big|_i = \frac{u_{i+1} - u_{i-1}}{2\Delta x} \tag{A.9}$$

Bibliography

[1] Smith, A.M.O., and Clutter, D. W :"Machine Calculation of Compressible Boundary Layers," *AIAA Journal*, vol. 3, no. 4, April 1965, pp. 639-647.

[2] Blottner, F.G :"Finite Difference Methods of Solution of the Boundary -Layer Equations ," *AIAA Journal*, vol. 8, no. 2, February 1970, pp. 193-205.

[3] DiCristina, V.:"Three-Dimensional Laminar Boundary-Layer Transition on a Sharp 8deg Cone at Mach 10," *AIAA Journal*, vol. 8, no. 5, May 1970, pp. 852-856.

[4] Stetson, K. F.:"Mach 6 Experiments of Transition a Cone at Angle of Attack ," *Journal of Spacecraft and Rockets*, vol. 19, no. 5, September-October 1982, pp. 397-403.

[5] Davis, R. T.:"Numerical Solution of Hypersonic Viscous Shock-Layer Equations ," *AIAA Journal*, vol. 8, no. 5, May 1970, pp. 843-851.

[6] McWherler, Mary, R. W. Naock, and Oberkampf, W. L:"Evaluation of Boundary-Layer and Parabolized Navier-Stokes Solutions for Re-entry Vehicles ," *Journal of Spacecrafts and Rockets*, vol. 23, no. 1, January-February 1986, pp. 70-78.

[7] Maccormack. R. W.:"Numerical Solution of Hypersonic Viscous Shock-Layer Equations ," *AIAAPaper*, vol. 8, no. 5, May 1969, pp. 843-851.

[8] Hays, W. and Probstein, R.:"Hypersonic Flow Theory" (Academic Press Inc., New York 1959), 1st ed., Chap. 4.

[9] Rasmussen, M. L: "On Hypersonic Flow Past an Unyawed Cone ," *AIAA Journal*, vol. 5, no. 8, August 1967, pp. 149-151.

[10] Daty, R. T and Rasmussen, M. L: "On Hypersonic Flow Past an Unyawed Cone ," *AIAA Journal*, vol. 5, no. 8, August 1967, pp. 149-151.

[11] Moretti, G. and M. Abbett: "A Time-Dependent Computational Method for Blunt-Body Flows ," *AIAA Journal*, vol. 4, no. 12, April 1966, pp. 2136-2141.

[12] MacCormack, R. W.: "A Numerical Methods for Solving the Equations of Compressible Viscous Flows ," *AIAA Journal*, vol. 20, no. 9, September 1982, pp. 1275-1281.

[13] Horstman, C. C.: "Hypersonic Shock-Wave/Turbulent-Boundary-Layer Interaction Flows ," *AIAA Journal*, vol. 30, no. 6, June 1992, pp. 1480-1481.

[14] Lind, C. A. and Lewis, M. J.: "Unsteady Characteristics of a Hypersonic Type IV Shock Interaction ," *Journal of Aircraft*, vol. 32, no. 6, November-December 1995, pp. 1286-1293.

[15] Gupta, R. N., Lee, Kam-Pui and Zoby, E. V., Moss, J. N and Thompson, R. A: "Enhancements to Viscous-Shock-Layer Technique ," *Journal of Spacecrafts and Rockets*, vol. 27, no. 2, March-April 1990, pp. 175-184.

[16] Kussoy, M. I., Horstman, K. C. and Horstman, C. C.: "Hypersonic Crossing Shock-Wave/Turbulent-Boundary-Layer Interactions ," *AIAA Journal*, vol. 31, no. 12, December 1993, pp. 2197-2203.

[17] Gupta, R. N., Lee, Kam-Pui and Zoby, E. V.: "Enhancements to Viscous-Shock-Layer Technique ," *Journal of Spacecrafts and Rockets*, vol. 30, no. 4, July-August 1993, pp. 404-412.

[18] Cheatwood, F. M. and DeJarnette, F. R.: "Approximate Viscous Shock Layer Technique for Calculating Hypersonic Flows About Blunt-Nosed Bodies ,"

Journal of Spacecrafts and Rockets, vol. 31, no. 4, July-August 1994, pp. 621-628.

[19] Bigdeli, B. and Lu, F. K.: "Hypersonic, Turbulent Viscous Interaction Past an Expansion Corner ," *AIAA Journal*, vol. 32, no. 9, September 1994, pp. 1815-1819.

[20] Luca de, L., Cardone, G., Chevalerie, D. A. de la,and Fonteneau, A.: "Viscous Interaction Phenomena in Hypersonic Wedge Flow ," *AIAA Journal*, vol. 33, no. 12, December 1995, pp. 2293-2298.

[21] Tannehill, J. C., Venkatapathy, E. and Rakich, J. V. : "Numerical Solution of Supersonic Viscous Flow over Blunt Delta Wings ," *AIAA Journal*, vol. 20, no. 2, February 1982, pp. 203-210.

[22] Barnett, M and Davis, T:" Calculation of Supersonic Flows with Storng Viscous-Inviscid Interaction "*AIAA Journal*, vol. 24, no. 12, December 1986, pp. 1949-1955.

[23] Dash, S. M., Wolf, D. E. and Sinha, N.:"Parabolized Navier-Stokes Analysis of Three-Dimensional Supersonic and Subsonic Jet Mixing Problems ," *AIAA Journal*, vol. 24, no. 8, August 1986, pp. 1252-1253.

[24] Kimmel, R. L., Klein, M. A. and Schwoerke, S. N.: "Three Dimensional Hypersonic Laminar Boundary-Layer Computations for Transition Experiment Design ," *Journal of Spacecrafts and Rockets*, vol. 34, no. 4, July-August 1997, pp. 409-414.

[25] Kumar, A. and Salas, M. D. : "Euler and Navier-Stokes Solutions for Supersonic Shear Flow past a Circular Cylinder ," *AIAA Journal*, vol. 23, no. 4, April 1985, pp. 583-587.

[26] Ching-Mao Hung and Barth, T. J : "Euler and Navier-Stokes Solutions for Supersonic Shear Flow past a Circular Cylinder ," *AIAA Journal*, vol. 28, no. 2, February 1990, pp. .

[27] Shang, J. S. and Scherr, S. J.:"Navier-Stokes Solution for a Complete Re-Entry Configuration ," *Journal of Aircraft*, vol. 23, no. 12, December 1986, pp. 881-887.

[28] Gupta, R. N., Lee, Kam-Pui and Zoby, E. V.:"Hypersonic Nonequilibrium Viscous Solutions over Slender Bodies ," *Journal of Spacecrafts and Rockets*, vol. 28, no. 3, May-June 1991, pp. 358-360.

[29] Oberkampf, W. L. and Aeschliman, D. P. : "Joint Computational/Experimental Aerodynamics Research on a Hypersonic Vehicle, Part 1: Experimental Results ," *AIAA Journal*, vol. 30, no. 8, August 1992, pp. 2000-2009.

[30] Walker, M. M. and Oberkampf, W. L. : "Joint Computational/Experimental Aerodynamics Research on a Hypersonic Vehicle, Part 2: Computational Results ," *AIAA Journal*, vol. 30, no. 8, August 1992, pp. 2010-2015.

[31] Lockman, W. K., Lawrence, S. L. and Cleary, J. W.: "Flow over an All-Body Hypersonic Aircraft: Experiment and Computation ," *Journal of Spacecrafts and Rockets*, vol. 29, no. 1, January-February 1992, pp. 7-14.

[32] Papuccuoglu, H. : "Experimental Investigation of Hypersonic Three-Dimensional Corner Flow ," *AIAA Journal*, vol. 31, no. 4, April 1993, pp. 652-656.

[33] Tai, C. and Kao. A.:"Navier-Stokes Solver for Hypersonic Flow over a Slender Cone ," *Journal of Spacecrafts and Rockets*, vol. 31, no. 2, March-April 1994, pp. 215-221.

[34] Kim, M. S.. Loellbach, J. M. and Lee, K. D.:"Effects of Gas Models on Hypersonic Base Flow Calculations ," *Journal of Spacecrafts and Rockets*, vol. 31, no. 2, March-April 1994, pp. 223-230.

[35] Morgenstern, A. Jr.and Chokani, N. : "Hypersonic Flow Past Open Cavities ," *AIAA Journal*. vol. 32, no. 12, December 1994, pp. 2387-2393.

[36] Mallet, E. R., Pullin, D. I. and Macrossan, M. N. : "Numerical Study of Hypersonic Leeward Flow over a Blunt Nosed Delta Wing ," *AIAA Journal*, vol. 33, no. 9, September 1995, pp. 1626-1633.

[37] Kopriva, D. A. : "Spectral Solution of the Viscous Blunt-Body Problem 2:Multidomain Approximation ," *AIAA Journal*, vol. 34, no. 3, March 1996, pp. 560-564.

[38] Yahia, D and Habashi, W. G. : "Finite Element Adaptive Method for Hypersonic Thermochemical·Nonequilibrium Flows ," *AIAA Journal*, vol. 35, no. 8, August 1997, pp. 1294-1301.

[39] Anderson, J. D.:"Hypersonic and High Temperature Gas Dynamics" (McGraw-Hill Book Co. 1984).

[40] Anderson, J. D.:"Computational Fluid Dynamics"McGraw-Hill Book Co. 1994).

[41] Anderson, D. A. and Tannehill, J. C.:"Computational Fluid Mechanics and Heat Transfer" (Hemisphere Publishing Co./McGraw-Hill Book Co. 1984).